population attributable fraction of 62.0% for hepato-cellular carcinoma cases with HCV infection was highest, and hepatocellular carcinoma cases with HBV infection, alcohol consumption of ≥40 g of ethanol per day, or obesity had population attributable fractions in the range of 13.4% to 20.1%. These are only approximate estimates of the potential for reducing hepatocellular carcinoma occurrence, as we do not know what effect removal of one risk factor would have on the distribution of the other risk factors.

Multivariate analysis after adjusting for severity of liver fibrosis indicated that hepatocellular carcinoma risk for HBV and HCV infections significantly decreased, which is consistent with the existing notion that hepato-cellular carcinoma risk increases with progression from chronic hepatitis B and C to liver cirrhosis. A large-scale meta-analysis (34) and a case-control study (35) showed a combined effect of HBV and HCV infections on hepato-cellular carcinoma risk, whereas our study did not detect similar effects among those with HBV+/HCV+ status. This difference may be partly attributable to the extremely limited number of coinfected subjects with HBV and HCV among our study population. It may be also partly because most past epidemiologic studies have defined chronic HCV infection by either anti-HCV antibody positivity or by HCV RNA positivity in serum (34, 35).

Several epidemiologic studies and clinical trials revealed an association between obesity and hepato-cellular carcinoma risk (9-12), but few population-based cohort studies have been conducted with precise adjustment for HBV and HCV infection status, the major risk factors for hepatocellular carcinoma. Obesity was recently found to be one of the etiologic factors for non-alcoholic steatohepatitis, which is considered a non-B, non-C liver disease, and it has been shown to be a risk factor for hepatocellular carcinoma (12, 16). Although many clinical studies showed that, among chronic hepatitis C patients, obesity was associated with pro-gression of inflammation, insulin resistance, hepatic steatosis, and liver fibrosis (17, 36), a study by Nair et al. (12) reported that obesity was not an independent risk factor for hepatocellular carcinoma among liver cirrhosis patients with HBV and HCV. On the other hand, a recent Western cohort study showed that being over-weight (BMI, 25 to <30 kg/m²) or obese (BMI, ≥30 kg/m²) was an independent risk factor for hepatocellular carcinoma (37).

In the present study, we adjusted for potentially confounding factors including hepatitis virus infection and also found that being obese 10 years before hepatocellular carcinoma diagnosis was associated with a 4.57-fold increase in hepatocellular carcinoma risk. Furthermore, we observed a statistically significant, positive, multiplicative interaction between HCV infec-tion and increased BMI on the risk for hepatocellular carcinoma, which indicates decisively that the joint effect of the two factors is greater than additive.

Obesity contributes to a high rate of visceral fat storage, accelerating production of tumor necrosis factor-α, interleukin 6, resistin, and leptin, and decreas-ing production of adiponectin (16). These cytokines presumably foster insulin resistance (16), cause hepatic steatosis and oxidative stress, and eventually promote hepatocellular carcinoma occurrence. A large number of studies pointed out association between progression of

Table 5. Interaction between hepatitis virus infection status and increase of BMI on hepatocellular carci-noma risk (joint hepatitis virus/BMI)

Viral etiology	BMI (kg/m²)	RR* (95% CI)[†]	Likelihood ratio P[†]
HBV−/HCV−	+1	1.05 (0.95-1.17)	0.33
HBV+/HCV−	+1	0.89 (0.64-1.23)	0.50
HBV−/HCV+	+1	1.39 (1.11-1.83)	0.003[‡]
HBV+/HCV+	+1	—[§]	—[§]

*Adjusted for continuous alcohol consumption, smoking habit, coffee drinking, diabetes mellitus, and radiation dose to the liver.
[†] Likelihood bounds and P values for relative risks estimated separately within each BMI/hepatitis virus category.
[‡] A quadratic term was also significant for HBV−/HCV+ individuals (P = 0.013). However, only the relative risk for the linear model in continuous BMI is shown because it is not possible to express the risk as a single value with a two-parameter linear-quadratic model.
[§] Neither could the joint effect of obesity and simultaneous HBV+/HCV+ status be estimated because of small numbers of jointly affected cases and controls.

liver fibrosis and insulin resistance or hepatic steatosis (15-17), but authenticity of any connection is now being questioned (8, 36). Interestingly, in this study, obesity remained an independent risk factor for hepatocellular carcinoma even after adjusting for all confounding factors including severity of liver fibrosis. The following are the possible reasons why obesity increases hepato-cellular carcinoma risk irrespective of severity of liver fibrosis: Several animal experiments showed that liver tumors were not always accompanied by advanced fibrosis among a variety of genetically engineered mouse models with steatohepatitis (38), and some reports indicated several nonalcoholic steatohepatitis–derived human cancer cases without significant liver fibrosis (39). The findings suggest that significant liver fibrosis is not essential for the carcinogenic process, but that steato-hepatitis itself is a state conferring a risk for high carcinogenicity. With regard to the proven relationship between obesity and such malignant tumors as colon, breast, and ovarian cancers (10), the cell proliferation activity of insulin due to hyperinsulinemia is believed to play a role in a common carcinogenic mechanism (5).

It is well documented that obesity induces insulin resistance, with a tendency to cause diabetes mellitus. In the case of hepatic cirrhosis accompanied by highly advanced liver fibrosis, glucose intolerance tends to lead to diabetes mellitus. A recent animal experiment showed that HCV contributed to progression of insulin resis-tance, resulting in diabetes mellitus (40). The present study failed to show that diabetes mellitus 10 years before hepatocellular carcinoma diagnosis was an inde-pendent risk factor for hepatocellular carcinoma, but an adjustment for all factors, except alcohol consumption and BMI, brought about a 30% increase in the effect of diabetes on hepatocellular carcinoma risk (data not shown). Such findings suggest a relationship between diabetes mellitus and alcohol consumption, as well as BMI. Therefore, by taking into account the proven association between alcohol consumption, obesity, and increased risk for hepatocellular carcinoma, our results will not likely refute an association between diabetes mellitus and hepatocellular carcinoma risk.

A large number of epidemiologic studies showed that heavy alcohol consumption was an independent risk factor for hepatocellular carcinoma and that there was

correlation between increased risk for hepatocellular carcinoma and amount of alcohol consumed (3, 9, 13, 14). In addition, in some case-control studies of hepatocellular carcinoma risk, synergistic interactions between alcohol consumption and hepatitis virus infection, or between obesity and diabetes mellitus, have been observed (9, 13, 14). In the present study, after adjusting for other factors such as hepatitis virus infection and BMI, alcohol consumption of ≥40 g of ethanol produced a 4.36-fold increase in hepatocellular carcinoma risk. A few recent case-control studies suggested that ethanol consumption of <50 to 60 g/d (41, 42) or alcohol exposure <1,500 gram-years (9) had protective effects on the progression of liver fibrosis and risk for developing hepatocellular carcinoma. Reasons for such discrepancy between our result and former reports are unclear, but factors such as gender, age, race (43), hereditary predisposition, and etiology of liver disease presumably affect the severity of alcohol-related liver diseases. Our study also showed that effects of alcohol consumption of ≥40 g of ethanol per day on hepatocellular carcinoma risk were reduced after adjusting for all confounding factors including severity of liver fibrosis. The finding suggests that alcohol consumption may contribute to hepatic carcinogenesis by enhancing oxidative stress and aggravating liver fibrosis.

As a result of recent assessments by the IARC, hepatocellular carcinoma has been positioned as a smoking-related malignant disease (44). However, it has yet to be determined whether smoking itself has direct hepatic carcinogenic effects or whether smoking contributes to hepatic carcinogenesis by way of progression of liver fibrosis. A case-control study showed that 4-aminobiphenyl DNA adducts contained in tobacco smoke are a liver carcinogen (45). In the present study, we adjusted for potential confounding factors including hepatitis virus infection and failed to detect significant smoking effects on hepatocellular carcinoma risk; however, a multivariate analysis that excluded hepatitis virus infection showed significant effects of smoking (data not shown). With adjustment for all factors including severity of liver fibrosis, effects of smoking on hepatocellular carcinoma risk were found to be marginally significant. These findings suggest the possibility that smoking, in conjunction with hepatitis virus infection, further enhances the risk for hepatocellular carcinoma and might directly contribute to the mechanism of liver carcinogenesis.

Several epidemiologic studies indicated the involvement of coffee in decreased alanine aminotransferase activity and γ-glutamyltransferase level, suppression of progression to liver cirrhosis, and inhibited development of hepatocellular carcinoma (18, 19). Such oxidation inhibitors as caffeine, coffee diterpenes, and chlorogenic acid are among candidate substances in coffee that potentially reduce the risk for hepatocellular carcinoma, and several animal experiments have shown that such substances have direct inhibitory effects on hepatic carcinogenesis (46). Adjusting for all potential confounding factors including hepatitis virus infection rendered the effects of coffee drinking on hepatocellular carcinoma risk marginally significant, whereas adjusting for all factors, except hepatitis virus infection, revealed significant effects of coffee drinking (data not shown). Furthermore, adjusting for all factors including severity

of liver fibrosis erased the effects of coffee drinking on hepatocellular carcinoma risk. These findings suggest that coffee drinking may somehow suppress liver fibrosis and thereby indirectly reduce hepatocellular carcinoma risk.

The main strengths of our study are its prospective cohort-based, nested case-control design, which minimized selection bias and provided for the use of stored sera and a wealth of epidemiologic information obtained before hepatocellular carcinoma diagnosis. Indeed, the distributions of HBV and HCV infection status among hepatocellular carcinoma cases and controls and mean age at diagnosis among hepatocellular carcinoma cases were similar to those in previous reports on Japanese populations (2, 4). Another major strength of our study is that it incorporated, in a strict and in-depth manner, HBV and HCV infection status and showed the interrelationship between these and numerous other epidemiologic factors. It is difficult and expensive to perform full cohort serum analyses, whereas the nested case-control design used here can provide substantial reductions in cost and effort with little loss of statistical efficiency.

The main limitation of our study is that the severity of liver fibrosis could not be classified into fibrosis stage of F0 to F4 based on liver specimens. We used platelet counts and type IV collagen concentrations as surrogate, but independent, markers of liver fibrosis. Previous reports showed a strong correlation between platelet count and fibrosis stage in the presence of chronic hepatitis C (47) and a close association between levels of type IV collagen, a basic component of the hepatic basal membrane, and severity of liver fibrosis. Another limitation of our study is the usage of sera that had been stored for long periods of time. Proteins and HCV RNA trend to degrade during prolonged storage of either frozen or freeze-dried sera. However, we minimized this degradative effect by the selection of matched controls relative to time and method of serum storage. Furthermore, we have previously shown that the freeze-dried sera are interchangeable with frozen sera in serologic and molecular biological detection of HBV and HCV (22, 25). Finally, some hepatocellular carcinoma cases had to be excluded because of nonavailability of stored sera. We did not detect any differences between included and excluded cases in terms of demographic variables or BMI.

In conclusion, HBV and HCV infection and obesity were independent risk factors for hepatocellular carcinoma, even after taking into account the severity of liver fibrosis. Moreover, the combination of HCV infection and increased BMI exerted a synergistic effect on the risk for hepatocellular carcinoma. Alcohol consumption of ≥40 g of ethanol per day was also an independent risk factor for hepatocellular carcinoma, likely contributing to the development of hepatocellular carcinoma through liver fibrosis. The radiation effect on hepatocellular carcinoma risk was shown to be marginally significant in univariate analysis; whether the radiation effect is confounded with other factors will be closely examined in a separate report. A precise understanding of the mechanism by which obesity contributes to development of hepatocellular carcinoma should lead to better therapeutic strategies, public health policies, and cost-effectiveness.

—540—

Acknowledgments

References

1. Yu MC, Yuan JM. Environmental factors and risk for hepatocellular carcinoma. Gastroenterology 2004;127:S72–8.
2. Kiyosawa K, Umemura T, Ichijo T, et al. Hepatocellular carcinoma: recent trends in Japan. Gastroenterology 2004;127:S17–26.
3. Aizawa Y, Shibamoto Y, Takagi I, Zeniya M, Toda G. Analysis of factors affecting the appearance of hepatocellular carcinoma in patients with chronic hepatitis C. A long term follow-up study after histologic diagnosis. Cancer 2000;89:53–9.
4. Ohishi W, Kitamoto M, Aikata H, et al. Impact of aging on the development of hepatocellular carcinoma in patients with hepatitis C virus infection in Japan. Scand J Gastroenterol 2003;38:894–900.
5. Gupta K, Krishnaswamy G, Karnad A, Peiris AN. Insulin: a novel factor in carcinogenesis. Am J Med Sci 2002;323:140–5.
6. El-Serag HB, Tran T, Everhart JE. Diabetes increases the risk of chronic liver disease and hepatocellular carcinoma. Gastroenterology 2004;126:460–8.
7. Inoue M, Iwasaki M, Otani T, Sasazuki S, Noda M, Tsugane S. Diabetes mellitus and the risk of cancer: results from a large-scale population-based cohort study in Japan. Arch Intern Med 2006;166: 1871–7.
8. Caldwell SH, Crespo DM, Kang HS, Al-Osaimi AM. Obesity and hepatocellular carcinoma. Gastroenterology 2004;127:S97–103.
9. Marrero JA, Fontana RJ, Fu S, Conjeevaram HS, Su GL, Lok AS. Alcohol, tobacco and obesity are synergistic risk factors for hepatocellular carcinoma. J Hepatol 2005;42:218–24.
10. Calle EE, Rodriguez C, Walker-Thurmond K, Thun MJ. Overweight, obesity, and mortality from cancer in a prospectively studied cohort of U.S. adults. N Engl J Med 2003;348:1625–38.
11. Oh SW, Yoon YS, Shin SA. Effects of excess weight on cancer incidences depending on cancer sites and histologic findings among men: Korea National Health Insurance Corporation Study. J Clin Oncol 2005;23:4742–54.
12. Nair S, Mason A, Eason J, Loss G, Perrillo RP. Is obesity an independent risk factor for hepatocellular carcinoma in cirrhosis? Hepatology 2002;36:150–5.
13. Hassan MM, Hwang LY, Hatten CJ, et al. Risk factors for hepatocellular carcinoma: synergism of alcohol with viral hepatitis and diabetes mellitus. Hepatology 2002;36:1206–13.
14. Yuan JM, Govindarajan S, Arakawa K, Yu MC. Synergism of alcohol, diabetes, and viral hepatitis on the risk of hepatocellular carcinoma in blacks and whites in the U.S. Cancer 2004;101:1009–17.
15. Ferrannini E. Insulin resistance, iron, and the liver. Lancet 2000;355: 2181–2.
16. Bugianesi E, McCullough AJ, Marchesini G. Insulin resistance: a metabolic pathway to chronic liver disease. Hepatology 2005;42: 987–1000.
17. Hu KQ, Kyulo NL, Esrailian E, et al. Overweight and obesity, hepatic steatosis, and progression of chronic hepatitis C: a retrospective study on a large cohort of patients in the United States. J Hepatol 2004;40:147–54.
18. Inoue M, Yoshimi I, Sobue T, Tsugane S; JPHC Study Group. Influence of coffee drinking on subsequent risk of hepatocellular carcinoma: a prospective study in Japan. J Natl Cancer Inst 2005;97: 293–300.
19. Ruhl CE, Everhart JE. Coffee and caffeine consumption reduce the risk of elevated serum alanine aminotransferase activity in the United States. Gastroenterology 2005;128:24–32.
20. Yaginuma K, Kobayashi H, Kobayashi M, Morishima T, Matsuyama K, Koike K. Multiple integration site of hepatitis B virus DNA in hepatocellular carcinoma and chronic active hepatitis tissues from children. J Virol 1987;61:1808–13.
21. Moriya K, Nakagawa K, Santa T, et al. Oxidative stress in the absence of inflammation in a mouse model for hepatitis C virus-associated hepatocarcinogenesis. Cancer Res 2001;61:4365–70.
22. Ohishi W, Fujiwara S, Suzuki G, et al. Feasibility of freeze-dried sera for serological and molecular biological detection of hepatitis B and C viruses. J Clin Microbiol 2006;44:4593–5.
23. Fukuhara T, Sharp GB, Mizuno T, et al. Liver cancer in atomic-bomb survivors: histological characteristics and relationships to radiation and hepatitis B and C viruses. J Radiat Res 2001;42:117–30.
24. Cologne JB, Sharp GB, Neriishi K, Verkasalo PK, Land CE, Nakachi K. Improving the efficiency of nested case-control studies of interaction by selecting controls using counter matching on exposure. Int J Epidemiol 2004;33:485–92.
25. Ohishi W, Fujiwara S, Suzuki G, Chayama K. Validation of the use of freeze-dried sera for the diagnosis of hepatitis B and C virus infections in a longitudinal study cohort. In: Mohan RM, editor. Research Advances in Microbiology 7. Kerala, India: Global Research Network; 2007. p. 1–9.
26. Sharp GB, Lagarde F, Mizuno T, et al. Relationship of hepatocellular carcinoma to soya food consumption: a cohort-based, case-control study in Japan. Int J Cancer 2005;115:290–5.
27. The World Health Organization Western Pacific Region; The International Association for the Study; The International Obesity Task Force. The Asia-Pacific perspective: redefining obesity and its treatment. Sydney, Australia: Health Communications Australia Pty Limited; 2000.
28. Young RW, Kerr GD, editors. Reassessment of the atomic bomb radiation dosimetry for Hiroshima and Nagasaki, Dosimetry System 2002, Report of the Joint US-Japan Working Group. Hiroshima, Japan: Radiation Effects Research Foundation; 2005.
29. Langholz B, Borgan Ø. Counter-matching: a stratified nested case-control sampling method. Biometrika 1985;82:69–79.
30. Breslow NE, Day NE. Statistical methods in cancer research: volume 1—the analysis of case-control studies. Lyon: IARC; 1980.
31. Cologne JB, Shibata Y. Optimal case-control matching in practice. Epidemiology 1995;6:271–5.
32. Cologne J, Langholz B. Selecting controls for assessing interaction in nested case-control studies. J Epidemiol 2003;13:193–202.
33. Cologne JB, Tokuoka S, Beebe GW, Fukuhara T, Mabuchi K. Effects of radiation on incidence of primary liver cancer among atomic bomb survivors. Radiat Res 1999;152:364–73.
34. Donato F, Boffetta P, Puoti M. A meta-analysis of epidemiological studies on the combined effect of hepatitis B and C virus infections in causing hepatocellular carcinoma. Int J Cancer 1998;75:347–54.
35. Kirk GD, Lesi OA, Mendy M, et al. The Gambia Liver Cancer Study: Infection with hepatitis B and C and the risk of hepatocellular carcinoma in West Africa. Hepatology 2004;39:211–9.
36. Perumalswami P, Kleiner DE, Lutchman G, et al. Steatosis and progression of fibrosis in untreated patients with chronic hepatitis C infection. Hepatology 2006;43:780–7.
37. Ioannou GN, Splan MF, Weiss NS, McDonald GB, Beretta L, Lee SP. Incidence and predictors of hepatocellular carcinoma in patients with cirrhosis. Clin Gastroenterol Hepatol 2007;5:938–45.
38. Fan CY, Pan J, Usuda N, Yeldandi AV, Rao MS, Reddy JK. Steatohepatitis, spontaneous peroxisome proliferation and liver tumors in mice lacking peroxisomal fatty acyl-CoA oxidase. Implications for peroxisome proliferator-activated receptor α natural ligand metabolism. J Biol Chem 1998;273:15639–45.
39. Bullock RE, Zaitoun AM, Aithal GP, Ryder SD, Beckingham IJ, Lobo DN. Association of non-alcoholic steatohepatitis without significant fibrosis with hepatocellular carcinoma. J Hepatol 2004;41:685–6.
40. Shintani Y, Fujie H, Miyoshi H, et al. Hepatitis C virus infection and diabetes: direct involvement of the virus in the development of insulin resistance. Gastroenterology 2004;126:840–8.
41. Donato F, Tagger A, Gelatti U, et al. Alcohol and hepatocellular carcinoma: the effect of lifetime intake and hepatitis virus infections in men and women. Am J Epidemiol 2002;155:323–31.
42. Monto A, Patel K, Bostrom A, et al. Risks of a range of alcohol intake on hepatitis C-related fibrosis. Hepatology 2004;39:826–34.
43. Iwahashi K, Matsuo Y, Suwaki H, Nakamura K, Ichikawa Y. CYP2E1 and ALDH2 genotypes and alcohol dependence in Japanese. Alcohol Clin Exp Res 1995;19:564–6.
44. IARC. IARC Monographs on the evaluation of the carcinogenic risks to humans. Volume 83: tobacco smoke and involuntary smoking. Lyon: IARC; 2004.
45. Wang LY, Chen CJ, Zhang YJ, et al. 4-Aminobiphenyl DNA damage in liver tissue of hepatocellular carcinoma patients and controls. Am J Epidemiol 1998;147:315–23.
46. Tanaka T, Nishikawa A, Shima H, et al. Inhibitory effects of chlorogenic acid, reserpine, polyprenoic acid (E-5166), or coffee on hepatocarcinogenesis in rats and hamsters. Basic Life Sci 1990;52:429–40.
47. Pohl A, Behling C, Oliver D, Kilani M, Monson P, Hassanein T. Serum aminotransferase levels and platelet counts as predictors of degree of fibrosis in chronic hepatitis C virus infection. Am J Gastroenterol 2001;96:3142–6.

Biochemical analysis of human PIF1 helicase and functions of its N-terminal domain

Yongqing Gu[1,2], Yuji Masuda[1] and Kenji Kamiya[1,*]

[1]Research Institute for Radiation Biology and Medicine, Hiroshima University, Hiroshima 734-8553, Japan and [2]School of Medicine, Shihezi University, Shihezi, Xinjiang 832002, China

ABSTRACT

The evolutionary conserved PIF1 DNA helicase family appears to have largely nonoverlapping cellular functions. To better understand the functions of human PIF1, we investigated biochemical properties of this protein. Analysis of single-stranded (ss) DNA-dependent ATPase activity revealed nonstructural ssDNA to greatly stimulate ATPase activity due to a high affinity for PIF1, even though PIF1 preferentially unwinds forked substrates. This suggests that PIF1 needs a ssDNA region for loading and a forked structure for translocation entrance into a double strand region. Deletion analysis demonstrated novel functions of a unique N-terminal portion, named the PIF1 N-terminal (PINT) domain. When the PINT domain was truncated, apparent affinity for ssDNA and unwinding activity were much reduced, even though the maximum velocity of ATPase activity and K_m value for ATP were not affected. We suggest that the PINT domain contributes to enhancing the interaction with ssDNA through intrinsic binding activity. In addition, we found DNA strand-annealing activity, also residing in the PINT domain. Notably, the unwinding and annealing activities were inhibited by replication protein A. These results suggest that the functions of PIF1 might be restricted with particular situations and DNA structures.

INTRODUCTION

Helicases are ubiquitous enzymes that catalyze the unwinding of DNA duplexes using ATP as their energy source. They therefore play vital roles in nearly all DNA metabolic processes, including DNA replication, recombination and repair. The PIF1 subfamily of 5′–3′ DNA helicases (1–10) belongs to the SFI superfamily, conserved in diverse organisms (11).

In *Saccharomyces cerevisiae* (*Sc*), *Sc*Pif1 was originally identified because of its involvement in recombination

of mitochondrial DNA (mtDNA) (12,13). Dysfunction of *Sc*Pif1 leads to mitochondrial genetic instability due to spontaneous oxidative damage (14–16), and induces mtDNA damage (17). *Sc*Pif1p has not only mitochondrial targeting but also nuclear targeting signals and therefore is localized in both the mitochondria and nucleus (18). Nuclear *Sc*Pif1p has multiple functions. When it is over-produced, telomeres become shorter, while they elongate when it is eliminated (18,19). In the absence of nuclear *Sc*Pif1, gross chromosome rearrangement is also increased, and healing of double-stranded broken ends via telomere addition increases ~200- to 1000-fold. These data suggest a negative regulatory role of *Sc*Pif1 in telomere metabolism (18–24). Indeed, *Sc*Pif1 catalytically inhibits telomerase activity *in vitro* (25). Other genetic data suggest that *Sc*Pif1 plays roles in Okazaki fragment processing (26), pausing of replication progression at ribosomal DNA loci (27) and unwinding of hemicatenans (28).

Schizosaccharomyces pombe encodes a PIF1 homolog, Pfh1 (8,10) which is required for cell cycle progression in late *S*-phase and for appropriate responses to DNA damage agents (8,10). It is also implicated in lagging strand DNA processing (7).

Previous biochemical studies of human PIF1 were performed using N-terminal-truncated forms of PIF1, containing only the conserved helicase motifs, located in the C-terminus, since it earlier proved impossible to obtain purified full-length human PIF1 protein (3,4,9). However, we found that the N-terminal region of human PIF1, named here as the PIF1 N-terminal (PINT) domain, is well conserved in the PIF1 family, suggesting a possible functional role. Here, we established a method to purify full-length human PIF1 protein and provided the first evidence that the PINT domain has crucial functions in this enzyme.

MATERIALS AND METHODS

Plasmid construction

The nucleotide sequence of the 5′-end of human PIF1 cDNA was obtained by 5′-rapid amplification of cDNA ends. Then the full-length human *PIF1* cDNA was

amplified from a HeLa cDNA library using primers, CATATGCTCTCGGGCATAGAGGCGGCGGCAGG GGAATATGAGGACTCG and TCAGAGGATTGGG TCCATGTT by PCR, then the nucleotide sequences of the clones were verified and submitted to the database with the accession number, EU084033. The entire coding region with a histidine tag at the N-terminus was inserted into the pET20b(+) vector to yield pET20b-PIF1. The truncated forms, PIF$^{167-641}$ and PIF$^{1-180}$ consisting of the numbered amino acid residues were also cloned into pET20b(+) and pET15b, respectively, to produce his-tagged fusion proteins. The structures of the resultant plasmids, pET20b-PIF1, pET20b-PIF$^{167-641}$ and pET15b-PIF$^{1-180}$, are shown in Supplementary Figure S1. In this article, PIF$^{167-641}$ and PIF$^{1-180}$ are referred to as C-terminal region of PIF1 (PIF1C) and N-terminal region of PIF1 (PIF1N), respectively.

Protein purification

RPA was purified as described (29) from over producing *Escherichia coli* cells (30). PIF1 and its deletion derivatives were purified as his-tagged fusion proteins at the N-termini. During all the purification steps, induced proteins were monitored by SDS–PAGE followed by staining with Coomassie Brilliant Blue R-250, or western blotting using Penta-His antibody (#34660, QIAGEN, Tokyo, Japan) or anti-PIF1 antibodies. Protein concentrations were determined by Bio-Rad protein assay using BSA (Bio-Rad, Tokyo, Japan) as the standard.

His-tagged full-length PIF1 and PIF1C were purified from overexpressing *E. coli* cells, BL21 (DE3) (31). The strain harboring a plasmid pMStRNA1, in which tRNAs for rare codons were cloned into a R6K derived kanamycin resistant plasmid (32), and pET20b-PIF1 was grown in 3 l of LB supplemented with ampicillin (250 µg/ml) and kanamycine (30 µg/ml) at 15°C, with aeration until the culture reached an A$_{600}$ value of 0.6. Isopropyl β-D-thiogalactopyranoside (IPTG) was added to 0.2 mM, and the incubation was continued for 14 h. The resultant cell paste (9 g) was resuspended in 18 ml of buffer I (50 mM HEPES NaOH pH 7.5, 0.1 mM EDTA, 10 mM β-mercaptoethanol, 1 M NaCl) and frozen in liquid nitrogen. The cells were thawed in ice water and lyzed by addition of 3 ml buffer I containing 100 mM spermidine and 4 mg/ml lysozyme. After incubation on ice for 30 min, heating in a 37°C water bath for 2 min and further incubation on ice for 30 min, the lyzate was clarified by centrifugation twice at 85 000g for 30 min at 4°C. Subsequent column chromatography was carried out at 4°C using a fast protein liquid chromatography (FPLC) system (GE Healthcare, Tokyo, Japan). After adding imidazole to 50 mM, the lyzate was applied at 0.2 ml/min to a 1-ml HiTrap chelating column (GE Healthcare), which had been treated with 0.1 M NiSO$_4$ and then equilibrated with buffer A (50 mM HEPES NaOH pH 7.5, 10% glycerol, 10 mM β-mercaptoethanol, 1 M NaCl) containing 50 mM imidazole. The column was washed with 10 ml of equilibration buffer at 0.2 ml/min and his-tagged PIF1 was eluted with 10 ml of buffer A containing 100 mM imidazole. Fractions eluted with 100 mM imidazole were pooled

and diluted to 50 mM imidazole with buffer A, then loaded again onto a 1-ml HiTrap chelating column at 0.2 ml/min. The column was washed, and PIF1 was eluted with buffer A containing 300 mM imidazole, then loaded at 0.1 ml/min onto a Superdex 200 10/300 GL column (GE Healthcare) equilibrated with buffer A. PIF1 peak fractions were pooled, frozen in liquid nitrogen, and stored at –80°C. His-tagged PIF1C was purified under the same conditions as described for his-tagged PIF1.

His-tagged human PIF1N was purified from overexpressing *E. coli* cells, Rosetta 2 (DE3) (Novagen, Tokyo, Japan). The strain harboring pET15-PIF1N was grown in 3 l of LB supplemented with ampicillin (250 µg/ml) and chloramphenicol (30 µg/ml) at 15°C with aeration until the culture reached an A$_{600}$ value of 0.6. IPTG was added to 0.2 mM, the incubation was continued for 14 h, and the cells were lyzated as described. After adding imidazole to 50 mM, the lyzate was applied at 0.2 ml/min to a 1-ml HiTrap chelating column, which had been treated with 0.1 M NiSO$_4$ and then equilibrated with buffer A containing 50 mM imidazole. The column was washed with 10 ml of equilibration buffer at 0.2 ml/min and then with 10 ml of buffer A containing 100 mM imidazole. His-tagged PIF1N was eluted with 10 ml of 300 mM imidazole in buffer A. Fractions containing PIF1N were pooled, diluted with buffer B (50 mM HEPES NaOH pH7.5, 10 mM β-mercaptoethanol) to 100 mM of NaCl, and applied at 0.5 ml/min to a 1-ml HiTrap SP HP column (GE Healthcare) equilibrated with buffer B containing 100 mM NaCl. The column was washed with 10 ml of equilibration buffer at 0.1 ml/min, and the PIF1N was eluted with 20 ml of a linear gradient of 100–1000 mM NaCl in buffer B. Fractions containing PIF1N were pooled, frozen in liquid nitrogen and stored at –80°C.

Antibodies

To obtain polyclonal antibodies against PIF1, truncated his-tagged PIF1 proteins (1–180 and 338–641 amino acids) were expressed in Rosetta 2 (DE3), purified and used to immunize rabbits.

DNA substrates

The oligonucleotides employed for the preparation of DNA substrates are listed in Table 1. Oligonucleotides were 5'-end labeled using [γ-^{32}P]ATP (GE Healthcare) and polynucleotide kinase (New England BioLabs, Tokyo, Japan). The schematic structures of substrates are shown in figures, and the labeled oligonucleotides are indicated with asterisks. Annealing reaction mixtures (30 µl) containing the 5'-^{32}P-labeled oligonucleotides at 1 µM, all unlabeled oligonucleotides at 3 µM, 10 mM Tris–HCl (pH 7.5), 7 mM MgCl$_2$ and 200 mM NaCl were heated at 95°C for 10 min, transferred directly to 65°C and held at that temperature for 1 h, slow-cooled to 25°C over a period of 2 h and held at that temperature for 30 min and then cooled to 4°C. Substrates were then purified by electrophoresis through 15–25% polyacrylamide using 0.5× TBE (33) as the electrophoresis buffer. Substrates were eluted from the gel by crushing the gel

slice in TE buffer and incubating overnight at 4°C. The slurry was then filtered through Micro Bio-Spin (Bio-Rad) columns, and the DNA was recovered by ethanol precipitation and resuspended in TE buffer.

ATPase assays

ATPase activity was measured in a standard reaction mixture (20 μl) containing 50 mM Tris–HCl (pH 8.0), 2 mM DTT, 1.2 mM MgCl$_2$, 0.25 mg/ml BSA, 2 mM [γ-^{32}P]ATP, indicated DNA and 1 μl of protein sample diluted with buffer D (50 mM Tris-HCl pH8.0, 1 M NaCl, 2 mM DTT, 10% glycerol, 0.1 mg/ml BSA) to obtain indicated final concentrations. After preincubation for 30 s at 30°C, reactions were initiated by the addition of PIF1 proteins and further incubated for 10 min. After the reaction was stopped with 4 μl of 20 mM EDTA (pH 8.0), an aliquot (2 μl) was spotted onto a polyethyleneimine-cellulose plate (Merck, Tokyo, Japan) and developed in 0.3 M LiCl/0.9 M formic acid. The products were analyzed using a Bio-Imaging Analyzer BAS2000 (Fuji Photo Film Co., Ltd., Tokyo, Japan). The extents of ATP hydrolysis were measured with reference to the relative ratios of radioactivity of inorganic phosphate to uncleaved ATP.

Kinetic assays to determine K_m values for ATP were performed for 10 min in 20 μl reaction mixtures using 14 nM of PIF1 and PIF1C with 3.8 μM and 150 μM (in nucleotides) of M13 mp7 single-stranded (ss) DNA, respectively. Concentrations of ATP ranged from 25 to 400 μM. K_m values were evaluated from the plot of the initial velocity versus the ATP concentration using a hyperbolic curve-fitting program with correlation coefficients (R^2) >0.99.

DNA helicase assays

DNA helicase activity was measured under ATPase assay conditions (20 μl) with the indicated DNA substrate (0.35 nM) and 1 μl of protein sample diluted with buffer D to obtain the indicated final concentrations. After preincubation for 30 s at 30°C, reactions were initiated by the addition of PIF1 proteins and incubated for 10 min at 30°C. Helicase reactions were terminated with 10 μl of stop solution (150 mM EDTA, 30% glycerol, 2% SDS, 0.1% bromophenol blue). In kinetic experiments, a 160-μl reaction mixture was incubated at 30°C and 10-μl aliquots were withdrawn at the indicated times. The reaction products were subjected to electrophoresis through 15–25% polyacrylamide gels in Tris–glycine buffer (33). The gels were dried on DE81 paper (Whatman, Tokyo, Japan) and autoradiographed. DNA products were quantified using a Bio-Imaging Analyzer.

Electrophoretic mobility shift assays

Oligonucleotides were labeled with polynucleotide kinase (New England BioLabs) and [γ-^{32}P]ATP. Assays of DNA binding were performed with a modification of a method described previously (34). The reactions (20 μl) were carried out under ATPase assay conditions, sometimes omitting MgCl$_2$ or ATP, with 25 pM oligonucleotides and 1 μl of protein sample diluted with buffer D to obtain the

indicated final concentrations. Incubation was carried out on ice for 10 min followed by loading on prerunning 5% polyacrylamide gels (79:1 acrylamide/bis-acrylamide). The electrophoresis buffer contained 6 mM Tris–HCl (pH 8.0), 5 mM sodium acetate and 1 mM EDTA, and the gels were subjected to a constant voltage of 8 V/cm for 100 min at 4°C. Following gel electrophoresis, the products were analyzed as described for the helicase assay. For quantification, fractions of free DNA were measured, and the binding fractions were determined by subtraction from the amount of the free DNA at 0 nM of the protein (35).

For RPA binding experiments, the reactions (20 μl) were carried out under the ATPase assay conditions, sometimes omitting ATP. The substrate 3F:4L (0.35 nM) was incubated, directly or after heating at 100°C for 5 min, with 1 μl of RPA sample diluted with buffer (50 mM HEPES NaOH pH 7.5, 250 mM NaCl, 10 mM β-mercaptoethanol, 10% glycerol) to obtain indicated final concentrations. Incubation was carried out on ice for 10 min, and the products were analyzed as in the PIF1 binding experiments.

DNA strand annealing assays

Strand annealing reactions (20 μl) were carried out under the ATPase assay conditions, but in the presence of the indicated concentrations of ATP, with the 5′-end labeled substrate DNA for helicase assay (0.35 nM), which had been boiled at 100°C for 5 min and quickly chilled on ice before adding to the reaction mixture, and 1 μl of protein sample diluted with buffer D to obtain the indicated final concentrations. After preincubation for 30 s at 30°C, reactions were initiated by the addition of PIF1 proteins, with incubation for 10 min at 30°C. After terminating the reactions with 10 μl of stop solution, the products were analyzed as described for the helicase assay. Kinetic experiments were also carried out as described for the helicase assay.

RESULTS

Purification of PIF1 protein and its deletion derivatives

Previously, biochemical studies of human PIF1 were performed using N-terminal-truncated forms of PIF1 containing only the conserved helicase motifs, located in the C-terminus (Supplementary Figure S2A). However, we found that the PINT domain is well conserved in the PIF1 family (Supplementary Figure S2B), suggesting that it plays a functional role. To examine biochemical activity, we established a procedure to purify full-length PIF1 with a 6× histidine tag at the N-terminus at quantities sufficient for detailed biochemical studies from overproducing *E. coli* cells (Supplementary Figure S2C). We also purified a C-terminal truncated form (PIF1N) and a N-terminal truncated form (PIF1C) (Supplementary Figure S2A) to address biochemical functions of individual domains. PIF1C and PIF1N consist of only the seven helicase motifs and only the PINT domain, respectively (Supplementary Figure S2A and Materials and methods section). Elution profiles from gel filtration chromatography

suggested PIF1 and PIF1C to be monomers (data not shown) as described in yeast homologs (1,5,7). The purified proteins were analyzed by SDS–PAGE followed by CBB staining and western blotting, showing PIF1, PIF1C and PIF1N to have molecular sizes of 71, 54 and 22 kDa, respectively (Supplementary Figure S2C).

Unwinding activities of PIF1 and PIF1C, a mutant lacking PINT domain but containing the helicase domain

We first measured DNA helicase activity of the purified proteins using the indicated DNA substrate (Figure 1A). When 5' overhang (1F:2S) and 3' overhang (1R:2S) DNA were used as substrates, we detected helicase activity only on the 5'-overhang substrate, consistent with previous reports (3,9), although the activity was very low (Figure 1B). In the titration experiment, activity was only detected clearly at the maximum concentration of the purified sample (Figure 1B). Since yeast PIF1 homologs preferentially unwind forked structures (1,5,7), we tested a forked substrate (Figure 1C). The titration experiment demonstrated that human PIF1 efficiently unwound the forked substrate with about 10 times higher activity than that for the 5'-overhang substrate (Figure 1C), suggesting that the property was conserved in evolution. Time course experiments using the forked substrate demonstrated that PIF1 could unwind up to 50% of the substrate in a 15 min reaction, although longer incubation did not increase the products (Figure 1D).

To compare the unwinding activity of PIF1C, titration experiments were performed with the forked substrate.

We found that PIF1C exhibited helicase activity, but it required more than 100 times more protein to obtain equivalent activity to that of PIF1 (Figure 1C). As a control, we showed that PINT domain itself could not unwind the substrate (Figure 1C). These results suggested that the function of the PINT domain could be enhancement of the unwinding activity of the helicase domain.

Nonstructural ssDNA, but not forked-structural DNA, preferentially stimulates ATPase activity of PIF1

DNA helicases are enzymes with an associated DNA-dependent ATPase activity. They are presumed to use the hydrolysis of ATP to translocate to ssDNA and to subsequently break the hydrogen bonds of duplex DNA. Characterization of ATPase activity could provide important information as a helicase. To analyze ssDNA dependent ATPase activity of PIF1, titration of M13 mp7 ssDNA was performed in reactions with optimal concentrations of ATP and $MgCl_2$ (Figure 2A). The result showed that the ATPase activity was increased depending on the concentrations of ssDNA and reached a plateau between 3 and 50 μM (in nucleotide equivalents) of ssDNA (Figure 2A). The maximum rate of ATP hydrolysis was calculated to be about 1 000 min^{-1}, which was equivalent to 5000 min^{-1} at 37°C of *Sc*Pif1 (5) and 4000 min^{-1} at 30°C of the fission yeast homolog, Pfh1 (7), which have been determined under reaction conditions with nearly saturated concentrations of ssDNA.

To describe precisely the concentration of ssDNA required for ATPase activity, a kinetic parameter,
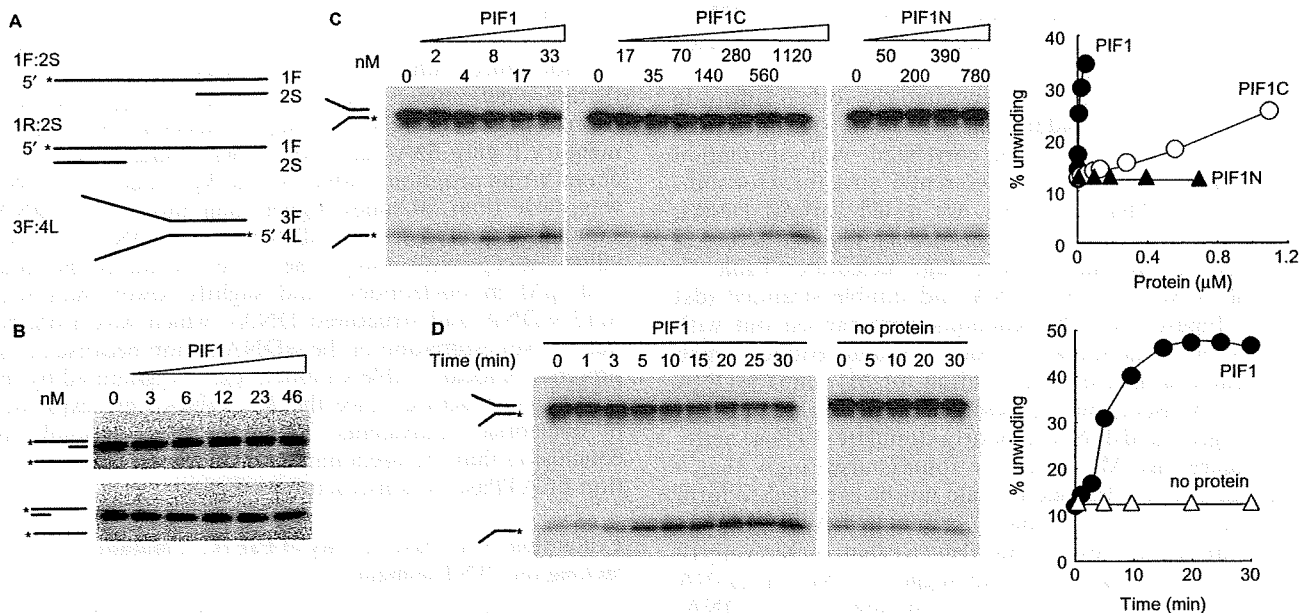
Figure 1. Helicase activity of PIF1. (**A**) Schematic structures of the DNA substrates. The asterisks indicate ^{32}P-labeled 5' phosphate. (**B**) Helicase activity of PIF1. Increasing levels of PIF1 were incubated with substrates (0.35 nM) with the 5'overhang, 1F:2S (upper panel), or 3' overhang, 1R:2S (lower panel) under standard reaction mixtures at 30°C for 10 min. Reaction products were separated on a 15–25% polyacrylamide gel. (**C**) Helicase activity of PIF1, PIF1N and PIF1C proteins. The forked structure partial duplex DNA substrate, 3F:4L (0.35 nM), was incubated with the indicated concentrations of PIF1, PIF1N and PIF1C under standard reaction conditions at 30°C for 10 min. The quantified data are shown graphically. The errors in the experiments were <10%. (**D**) Time course of unwinding reactions with PIF1. The forked structure partial duplex DNA substrate, 3F:4L (0.35 nM), was incubated at 30°C for the indicated time under standard reaction conditions with PIF1 (33 nM). The quantified data are shown graphically. The errors in the experiments were <10%.

Figure 2. Effects of various DNA molecules on stimulation of ATPase activity of PIF1. (**A**) Titration of M13 mp7 ssDNA for its stimulation of ATPase activity of PIF1, PIF1N and PIF1C. ATPase activities were measured under standard reaction conditions with PIF1 proteins (13.9 nM) at 30°C for 10 min. An aliquot (2 μl) of the reaction products was then analyzed by thin layer chromatography. The extent of ATP hydrolysis was measured by determining the relative radioactivity of the released inorganic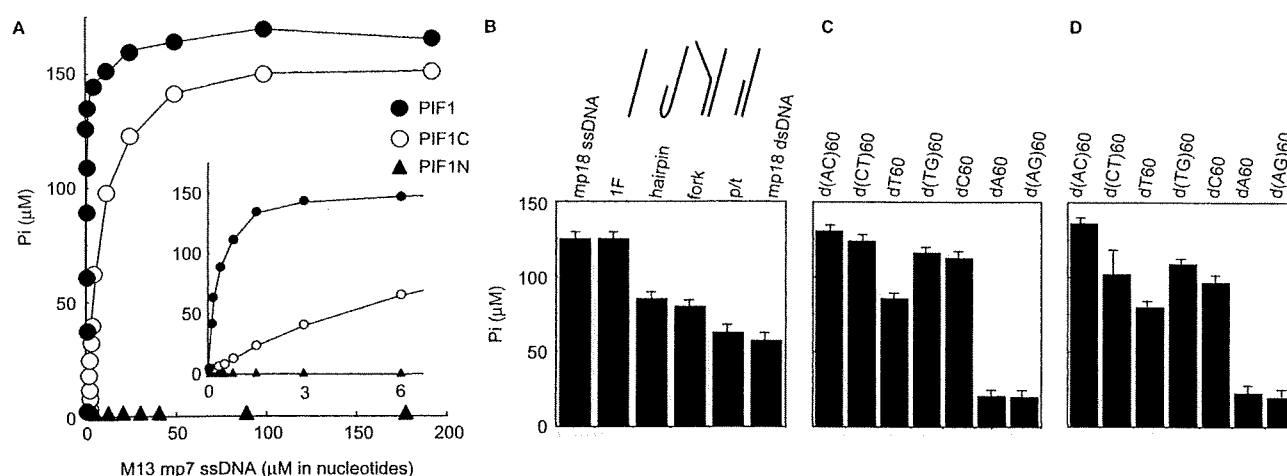 phosphate. Inset is a plot of the data at lower concentrations of ss DNA. The errors in the experiments were <10%. (**B**) Effects of the various DNA molecules on stimulation of ATPase activity of PIF1. Assays were performed with the indicated DNA (3.8 μM in nucleotides) and PIF1 (13.9 nM). (**C**) Effects of oligonucleotides with different compositions on stimulation of ATPase activity by PIF1. Assays were performed with indicated DNA (7.5 μM in nucleotides) and PIF1 (14.6 nM). (**D**) Effects of oligonucleotides with different compositions on stimulation of ATPase activity by PIF1C. Assays were performed with indicated DNA (150 μM in nucleotides), and PIF1C (13.9 nM).

K_{eff}, defined as the concentration of ssDNA required to achieve half-maximal ATP hydrolysis (5,36,37) was calculated from the titration curve (Figure 2A) using a hyperbolic curve-fitting program (Table 2). The calculated K_{eff} value, 0.35 μM (in nucleotides) for M13 mp18 ssDNA, agreed with the 0.6 μM (in nucleotides) of *Sc*Pif1 reported for the same M13 ssDNA (5).

Since PIF1 preferentially unwound the forked substrate (Figure 1), we consider that substrate specificity for unwinding activity could be correlated with stimulation of ATPase activity. To seek preferential structures for stimulation for ATPase of PIF1, we tested various DNAs, including a fork-structure, a primer-template-structure, a hairpin-structure and a linear oligonucleotide (Table 1), as well as M13 mp18 ssDNA and double stranded (ds) DNA (Figure 2B). The reactions were carried out with 3.8 μM (in nucleotides) of each oligonucleotide, which was nearly saturated concentration for M13 mp7 ssDNA (Figure 2A inset). Among these, M13 mp18 ssDNA proved to strongly and dsDNA to poorly stimulate ATPase activity (Figure 2B). Moreover, we found surprisingly that a oligonucleotide, 1F, which would not be expected to form secondary structures (Table 1), stimulated ATPase activity to the highest level, equivalent to that of M13 mp18 ssDNA (Figure 2B). The result suggested that an ssDNA region itself, rather than the structure of the DNA, is crucial for stimulation of ATPase activity of PIF1. Consequently, we compared ATPase activity stimulated by seven different 60-mer oligonucleotides composed of one or two nucleotides, guaranteed not to form secondary structures. The reactions were performed in the presence of a nearly saturated concentration of the oligonucleotides (7.5 μM in nucleotides) (Supplementary Figure S3A).

The results revealed general features of ssDNA for stimulation of ATPase (Figure 2C), with the order of stimulation being poly(purine–pyrimidine) ≥ polypyrimidine ≫ polypurine.

Since these experiments were performed with nearly saturated concentrations of oligonucleotides, the results do not reflect affinities of the respective ssDNAs. We therefore determined a kinetic parameter, K_{eff}, calculated from data of ssDNA-titration experiments (Supplementary Figure S3A, data not shown) using a hyperbolic curve-fitting program (Table 2). The K_{eff} value for dsDNA was more than 20 times higher than those for ssDNA, showing a preference to ssDNA. For ssDNA, the K_{eff} values, except with polypurine, were essentially the same (∼0.1 μM in nucleotides), and slightly lower than with M13 ssDNA and structured DNAs, which was probably due to over estimation of the ssDNA region because of the presence of local double-stranded regions generated by the secondary structure, since the K_{eff} values were expressed in nucleotide equivalents. These results supported our conclusion that the predominant requirement for stimulation of ATPase is nonstructural ssDNA.

Evaluation of ATPase activity of PIF1C, a mutant lacking the PINT domain

We noted that the K_{eff} value for ssDNA of PIF1 was in line with one report for *Sc*Pif1 (5), but significantly lower than that for human PIF1 with a N-terminal truncated form (4). We consider that the difference could be attributed to the missing function of the PINT domain. To test this possibility, we examined ATPase activity of PIF1C (Figure 2A), and also tested PIF1N as a control. First, we confirmed no ATPase activity of PIF1N (Figure 2A),

Table 1. Synthetic oligonucleotides used in this work

Name	Sequence
1F (73-mer)	5'-CTCCTCCTCCTCCTCCTCCTCCTCCTCCTCCTCCTCCTCCTCCTCGCTCGACGCCATTAATAAT GTTTTC-3'
1R (73-mer)	5'-GCTCGACGCCATTAATAATGTTTTCCTCCTCCTCCTCCTCCTCCTCCTCCTCCTCCTCCTCCTCCT CCTC-3'
2L (50-mer)	5'-GAAAACATTATTAATGGCGTCGAGCTAGGCACAAGGCGAACTGCTAACGG-3'
2S (25-mer)	5'-GAAAACATTATTAATGGCGTCGAGC-3'
3F (55-mer)	5'-AGGTCTCGACTAACTCTAGTCGTTGTTCCACCCGTCCACCCGACGCCACCTCCTG-3'
3S (25-mer)	5'-CCCGTCCACCCGACGCCACCTCCTG-3'
4S (25-mer)	5'-CAGGAGGTGGCGTCGGGTGGACGGG-3'
4L (51-mer)	5'-GCAGGAGGTGGCGTCGGGTGGACGGGATTGAAATTTAGGCTGGCACGGTCG-3'
5 (fork) (55-mer)	5'-TTTTTTTTTTTTTTTTTTTTTTTTTCGGACGCCTCGACGCCATTAATAATGTTTTC-3'
7 (fork) (56-mer)	5'-TGAAAACATTATTAATGGCGTCGAGCGTCCGTTTTTTTTTTTTTTTTTTTTTTTTTT-3'
18 (hairpin) (73-mer)	5'-GCCTGCACGTGGCGATCGTTCGATCGCCACGTGCAGGCGCTGCTGCTGGCTCGACGCCATTAAT AATGTTTTC-3'
90 (p/t) (90-mer)	5'-TGGGCTCACGTGGTCGACGCTGGAGGTGATCACCAGATGATTGCTAGGCATGCTTTCCGCAA GAGAACGGGCGTCTGCGTACCCGTGCAG-3'
30 (p/t) (30-mer)	5'-CTGCACGGGTACGCAGACGCCCGTTCTT-3'
d(AC)60 (60-mer)	5'-ACACACACACACACACACACACACACACACACACACACACACACACACACACACACACAC-3'
d(AG)60 (60-mer)	5'-AGAGAGAGAGAGAGAGAGAGAGAGAGAGAGAGAGAGAGAGAGAGAGAGAGAGAGAGAGAG-3'
d(TG)60 (60-mer)	5'-TGTGTGTGTGTGTGTGTGTGTGTGTGTGTGTGTGTGTGTGTGTGTGTGTGTGTGTGTGTG-3'
d(CT)60 (60-mer)	5'-CTCTCTCTCTCTCTCTCTCTCTCTCTCTCTCTCTCTCTCTCTCTCTCTCTCTCTCTCTCT-3'
d(CT)55 (55-mer)	5'-TCTCTCTCTCTCTCTCTCTCTCTCTCTCTCTCTCTCTCTCTCTCTCTCTCTCTCTCT-3'
d(CT)45 (45-mer)	5'-TCTCTCTCTCTCTCTCTCTCTCTCTCTCTCTCTCTCTCTCTCTCT-3'
d(CT)35 (35-mer)	5'-TCTCTCTCTCTCTCTCTCTCTCTCTCTCTCTCTCT-3'
d(CT)30 (30-mer)	5'-CTCTCTCTCTCTCTCTCTCTCTCTCTCTCT-3'
d(CT)20 (20-mer)	5'-CTCTCTCTCTCTCTCTCTCT-3'
d(CT)15 (15-mer)	5'-TCTCTCTCTCTCTCT-3'
dC60 (60-mer)	5'-CCCCCCCCCCCCCCCCCCCCCCCCCCCCCCCCCCCCCCCCCCCCCCCCCCCCCCCCCCCC-3'
dA60 (60-mer)	5'-AAAAAAAAAAAAAAAAAAAAAAAAAAAAAAAAAAAAAAAAAAAAAAAAAAAAAAAAAAAA-3'
dT60 (60-mer)	5'-TTTTTTTTTTTTTTTTTTTTTTTTTTTTTTTTTTTTTTTTTTTTTTTTTTTTTTTTTTTT-3'

Table 2. Kinetic parameters for the ATPase activity of PIF1 with various ssDNAs

DNA	PIF1 K_{eff}[a] (µM)	PIF1C K_{eff} (µM)
M13 mp7 ssDNA	0.35	8.7
M13 mp18 ssDNA	0.45	–[b]
M13 mp18 dsDNA	9.7	–
1F[c]	0.17	–
hairpin (18)[c]	0.71	–
fork (5:7)[c]	0.39	–
p/t (90:30)[c]	0.80	–
d(AC)60[c]	0.13	3.7
d(CT)60[c]	0.11	2.3
d(TG)30[c]	0.12	3.4
dT60[c]	0.11	6.4
dC60[c]	0.07	2.3
dA60[c]	1.2	nd[d]
d(AG)60[c]	1.8	nd

Kinetic assays to determine K_{eff} values were performed for 10 min in 20 µl reaction mixtures using 14 nM of PIF1 and PIF1C. Concentrations of ssDNA ranged from 0.15 to 300 µM in nucleotides. K_{eff} values were evaluated from the plot of the initial velocity versus the nucleotide concentration using a hyperbolic curve-fitting program with the correlation coefficients (R^2) more than 0.97, which were shown in supplementary Figure S3.
[a]K_{eff} is expressed in nucleotides equivalents.
[b]Not determined.
[c]Nucleotide sequences were shown in Table 1.
[d]Not detected.

as expected from the lack of any ATPase motifs. When M13 mp7 ssDNA was titrated in the reaction with PIF1C, we detected similar levels of maximum ATPase activity at higher concentrations of ssDNA (Figure 2A),

suggesting that the helicase domain is sufficient to express ATPase activity. However, the required concentrations of ssDNA to achieve maximal activity were significantly increased (Figure 2A inset). The calculated K_{eff} value, 8.7 µM (in nucleotides) for M13 mp7 ssDNAs with PIF1C was more than 20 times higher than that for PIF1 (Table 2). This property was also demonstrated by determining K_{eff} values for different oligonucleotides (Table 2), calculated from data from ssDNA titration experiments (Supplementary Figure S3B). These results suggested that a defect in PIF1C could be in the binding to ssDNA, and the PINT domain could help interaction between the helicase domain and ssDNA.

To determine preferential nucleotide compositions for PIF1C stimulation of ATPase activity, it was measured using the same set of the oligonucleotides in the reactions with nearly saturated concentrations of the oligonucleotides (150 µM in nucleotides) (Supplementary Figure S3B). The results demonstrated that the preference of PIF1C was essentially identical to that of PIF1 (Figure 2C and D), suggesting that it is intrinsic to the helicase domain, the PINT domain not affecting this property.

For further comparison between PIF1 and PIF1C, we determined their K_m values for ATP in the reactions with saturating concentrations of M13 mp18 ssDNA, 3.8 and 150 µM (in nucleotides), respectively. The K_m values for ATP of both proteins were both 0.17 mM and essentially identical to the previously reported value of 0.2 mM for N-terminal-truncated human PIF1 (4). This result

suggested again that the helicase domain is sufficient to express ssDNA-dependent ATPase activity.

Characterization of ssDNA binding activities of PIF1 and PIF1C

It seemed that the apparent affinity to ssDNA for the helicase domain (PIF1C) was much lower than that for PIF1 in ATPase reactions. We considered that the defect might be attributed to binding ability to ssDNA. To measure DNA binding of PIF1 and PIF1C directly, we performed electrophoretic mobility shift assays (EMSA) using a oligonucleotide, d(AC)60 (Table 1) as a model substrate. It has been reported that this assay detects DNA–protein complexes in yeast and human PIF1 in an ATP-independent manner (7,9). Binding reactions were carried out under the optimal ATPase assay conditions, then products were loaded on gels as described in the

Materials and methods section. The titration experiment displayed PIF1–DNA complexes, which were increased depending on the concentration of PIF1 (Figure 3A). The apparent K_d, which is approximately equal to the protein concentration at which half the free DNA has become bound (35), was determined to be about 3 nM. This was in good agreement with the K_{eff} value of d(AC)60 for ATPase activity, because the 0.13 μM (in nucleotides) (Table 2) corrected for the concentration of the 60-mer oligonucleotide became 2 nM.

When PIF1C was tested, we could detect PIF1C–DNA complexes, but the affinity seemed much lower than that with PIF1, demonstrating a defect in ssDNA binding activity. When the point at which half the free DNA has become bound was extrapolated from the binding curve, the apparent K_d value was estimated at about 10 nM. However, the K_d value was not directly correlated with the K_{eff} value, since it was still 6 times lower than the
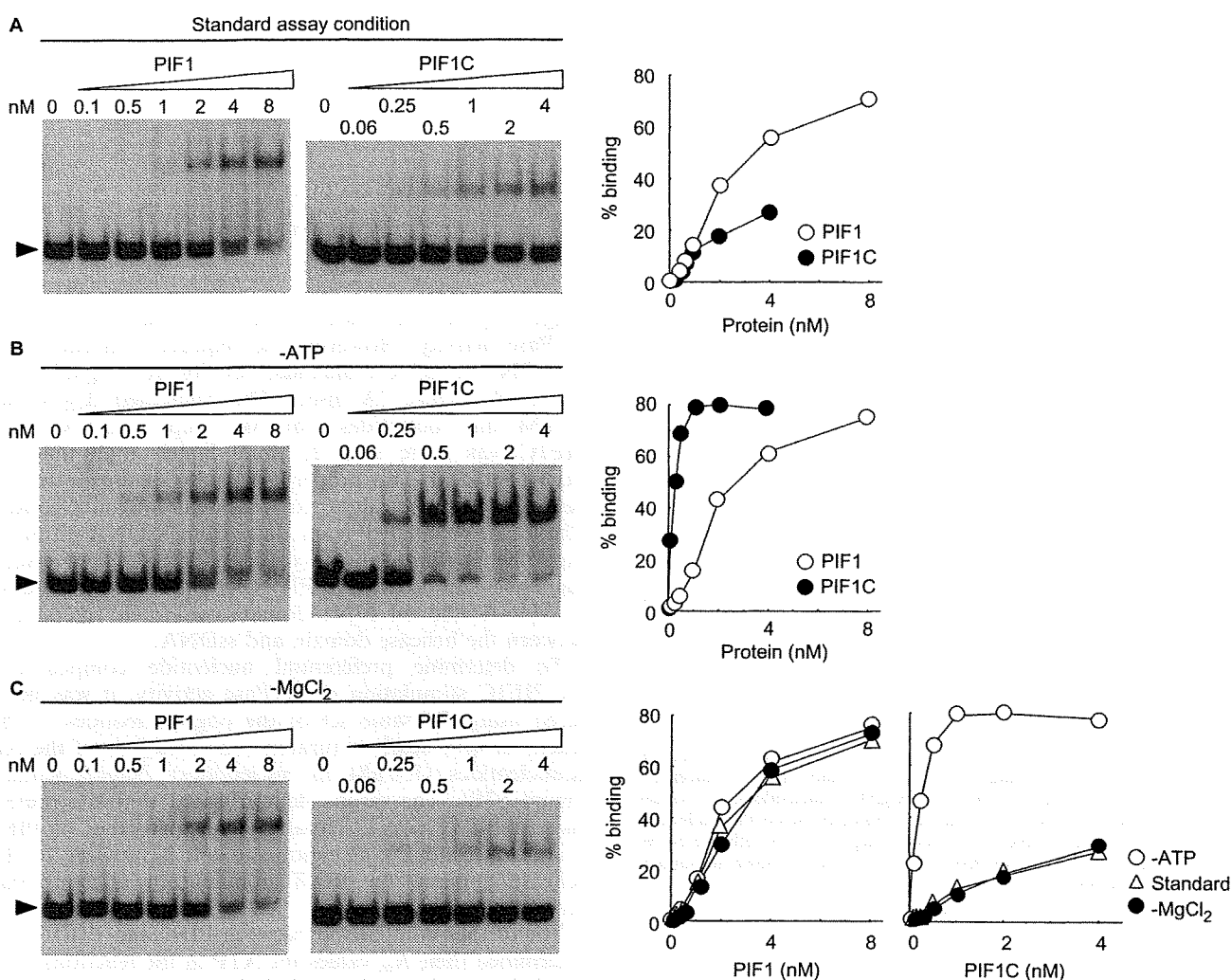
Figure 3. EMSA of PIF1 and PIF1C for binding to ssDNA. (A) EMSA of ssDNA binding to PIF1 and PIF1C under standard reaction conditions. The 5′-^{32}P labeled oligonucleotide, d(AC)60, was incubated with the indicated concentrations of PIF1. Arrowheads indicate the positions of free DNA. The quantified data are shown graphically. (B) EMSA in the absence of ATP. Experiments were performed as described in (A). The quantified data are shown graphically. (C) EMSA in the absence of MgCl$_2$. Experiments were performed as described in (A). The quantified data are shown graphically together with data from (A) and (B). The errors in the experiments were <10%.

apparent K_{eff} value of 60 nM (in oligonucleotides), with the K_{eff} value of 3.7 μM (in nucleotides) (Table 2), corrected for the concentration of the 60-mer oligonucleotide.

Since it was very likely that ATP could influence the binding reaction, we performed the same experiments without ATP. With the full length PIF1, the titration curve was not affected (Figure 3B). In contrast that for PIF1C in the absence of ATP was significantly changed. The apparent affinity was increased to about 0.3 nM (Figure 3B). To determine whether the effect of ATP is caused by binding or hydrolysis, titration experiments were carried out omitting $MgCl_2$ to prevent hydrolysis of ATP (Figure 3C). Under this condition, the ATPase activity was under the background level (data not shown), suggesting that, even though trace amounts of Mg ions were present as contaminants of chemicals, the contribution was negligible. The result clearly demonstrated the

binding curves to be identical to that under standard assay conditions containing ATP and $MgCl_2$ (Figure 3C), suggesting that ATP binding itself affected the interaction between ssDNA and the helicase domain.

ssDNA binding activity of the PIF1N

Our results suggested that the PINT domain plays a role in modulating the ssDNA binding activity of the helicase domain. Therefore, we carried out the same binding assays with PIF1N (Figure 4A). The assays detected PIF1N–DNA complexes, and the titration curves were not affected by ATP and $MgCl_2$ (Figure 4A), with an apparent K_d value of about 10 nM. These results suggested that PIF1N itself possesses ATP-independent ssDNA binding activity.

In contrast to the binding reactions with PIF1 and PIF1C shown in Figure 3, further shifts of the mobility
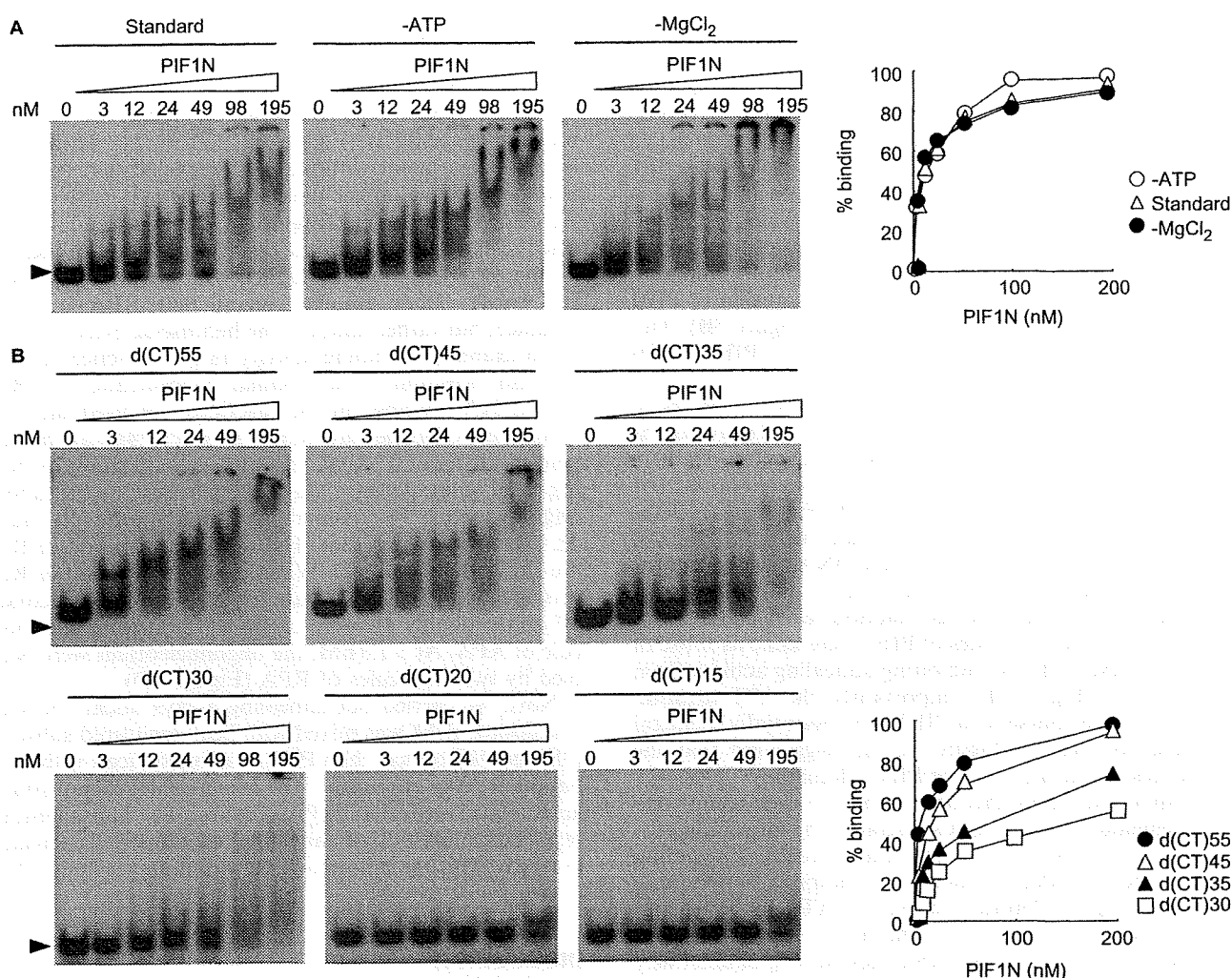
Figure 4. EMSA of PIF1N for binding to ssDNA. (A) Titration of PIF1N under different conditions. The $5'$-^{32}P labeled oligonucleotide, d(AC)60, was incubated with the shown concentrations of PIF1N, omitting ATP or $MgCl_2$ as indicated. Arrowheads indicate the positions of free DNA. The quantified data are shown graphically. (B) Binding ability of PIF1N to different sizes of oligonucleotides. Experiments were performed using indicated oligonucleotides as substrates under standard reaction conditions in the absence of ATP. The quantified data are shown graphically. The errors in the experiments were <10%.

of the complexes with PIF1N in higher concentrations were observed (Figure 4A). This could be due to more than one protein molecule binding to the 60-mer oligonucleotide. To determine the minimal ssDNA size for binding of PIF1N, six different oligonucleotides in lengths ranging from 55 to 15 bases were subjected to binding assays. When the 55-mer was used as the substrate, the result was essentially identical to that for a 60-mer. However, further reduction of the length to 45-mer and 35-mer decreased the extent of multiple binding. With the 30-mer oligonucleotide, but not the 20-mer and 15-mer, a distinct band of the complex was observed. These results demonstrated that the minimal ssDNA size could be between 30 and 20 bases.

DNA strand annealing activity of PIF1, residing in the PINT domain

During helicase assays, we unexpectedly found that PIF1 possessed robust annealing activity. For detailed analysis, a forked substrate (1F:2L) (Figure 5A) was denatured by heating at 100°C for 5 min, and then incubated with PIF1 under the conditions for the standard ATPase assay omitting ATP to avoid unwinding reactions. Titration of PIF1 showed about 50% of ssDNA could be annealed within 10 min when 46 nM PIF1 was present (Figure 5B). To determine the region of PIF1 responsible for the annealing activity, PIF1C and PIF1N were tested for their ability to promote the reaction. The results demonstrated that PIF1N, but not PIF1C, efficiently annealed ssDNA, with activity only 3-fold lower than that of PIF1 when 1F and 2L substrates were tested (Figure 5B). This result indicated that the annealing activity of PIF1 resides in the PINT domain.

Since ATP is essential for helicase activity, we tested effects of ATP on the annealing reaction. To avoid the effect of unwinding, titration of ATP was carried out in the absence of $MgCl_2$. The result demonstrated both PIF1 and PIF1N to be inhibited by ATP (Figure 5C). Time course experiments demonstrated that, in the absence of ATP, PIF1 annealed up to 70% of ssDNA, whereas, in the presence of the optimal concentration of ATP (2 mM) for helicase activity, the annealed fraction reached only 20% (Figure 5D). The properties of PIF1 were same as those of PIF1N, 2 mM ATP also inhibiting annealing activity from 50% to 17% (Figure 5E). Importantly, the ATP-titration curve and time course with PIF1 were essentially identical to those for PIF1N (Figure 5C–E), suggesting that the properties are intrinsic to the PINT domain.

Further confirming this conclusion, we used completely complementary strands as a substrate. The annealing product has no ssDNA region, preventing product unwinding under the standard reaction conditions containing ATP and $MgCl_2$. Titration curves of ATP for PIF1 and PIF1N demonstrated again inhibitory effects, although significant fractions of the substrates were spontaneously annealed under the assay conditions (Figure 5F).

Effects of RPA on unwinding and annealing reactions of PIF1

Elucidation of whether PIF1 has the potential to promote unwinding and annealing reactions on RPA-coated substrates is valuable for understanding cellular functions of PIF1. To do this, first, we determined the optimal concentration of RPA for the substrate DNA binding by EMSA. The substrate, 3F:4L was used for the binding reactions at the final concentration of 0.35 nM. The results of titration of RPA are shown in Figure 6A. When the concentration of RPA was increased to 0.9 nM, one molecule of RPA bound to at least one strand of the forked substrate. At >1.8 nM, each strand of the substrate was probably occupied by one RPA molecule (Figure 6A). The levels of apparent affinity of RPA for ssDNA were in good agreement with previous reports (38).

Then we examined unwinding activity of PIF1. RPA was mixed with the forked substrate, 3F:4L, under the standard reaction conditions on ice, then PIF1 was introduced and incubation was performed at 30°C for 10 min. We found that RPA did not affect unwinding reactions at low concentrations <0.4 nM (Figure 6B, left panel), in which majority of the substrate was RPA-free (Figure 6A). When the concentration of RPA reached 0.9 nM, at which almost all the oligonucleotides were occupied with RPA (Figure 6A), severe inhibition was observed (Figure 6B, left panel). At much higher concentrations of RPA, we observed unwinding products (Figure 6B, left panel). However, a control experiment without PIF1 revealed that the products detected at higher concentrations >1.8 nM of RPA were PIF1 independent (Figure 6B, right panel). The quantified results shown in Figure 6C demonstrate no difference in the two reactions at higher concentrations of RPA (>0.9 nM). These results suggest that RPA does not enhance, but rather inhibits, the helicase activity of PIF1.

To examine annealing activity in the presence of RPA, we also determined the optimal concentration of RPA for ssDNA binding. In the reactions, we used the same substrate as for the unwinding assay (3F:4L) at the final concentration of 0.35 nM, but after denaturation by heating. The assay detected only complexes with the labeled oligonucleotide 3F (55-mer), although another fragment, 4L (51-mer), was present. The results of titration of RPA are shown in Figure 6D. When the concentration of RPA was increased to 0.9 nM, almost all the oligonucleotides 3F and probably 4L were occupied by at least one molecule of RPA. At >1.8 nM, the oligonucleotides were occupied by two molecules of RPA (Figure 6D).

Next, we carried out annealing assays under the same conditions. RPA was mixed with heat denatured substrate (3F and 4L) on ice, then PIF1 was introduced with incubation at 30°C for 10 min. The result clearly demonstrated an inhibitory effect of RPA (Figure 6E). The quantified results for inhibition of annealing reactions well correlated inversely with the amount of RPA binding (Figure 6F).

DISCUSSION

In this article, we document for the first time the biochemical properties of full-length human PIF1 together with those of truncated forms consisting of individual domains. We could establish intrinsic properties of the helicase domain and functional roles of the PINT domain.
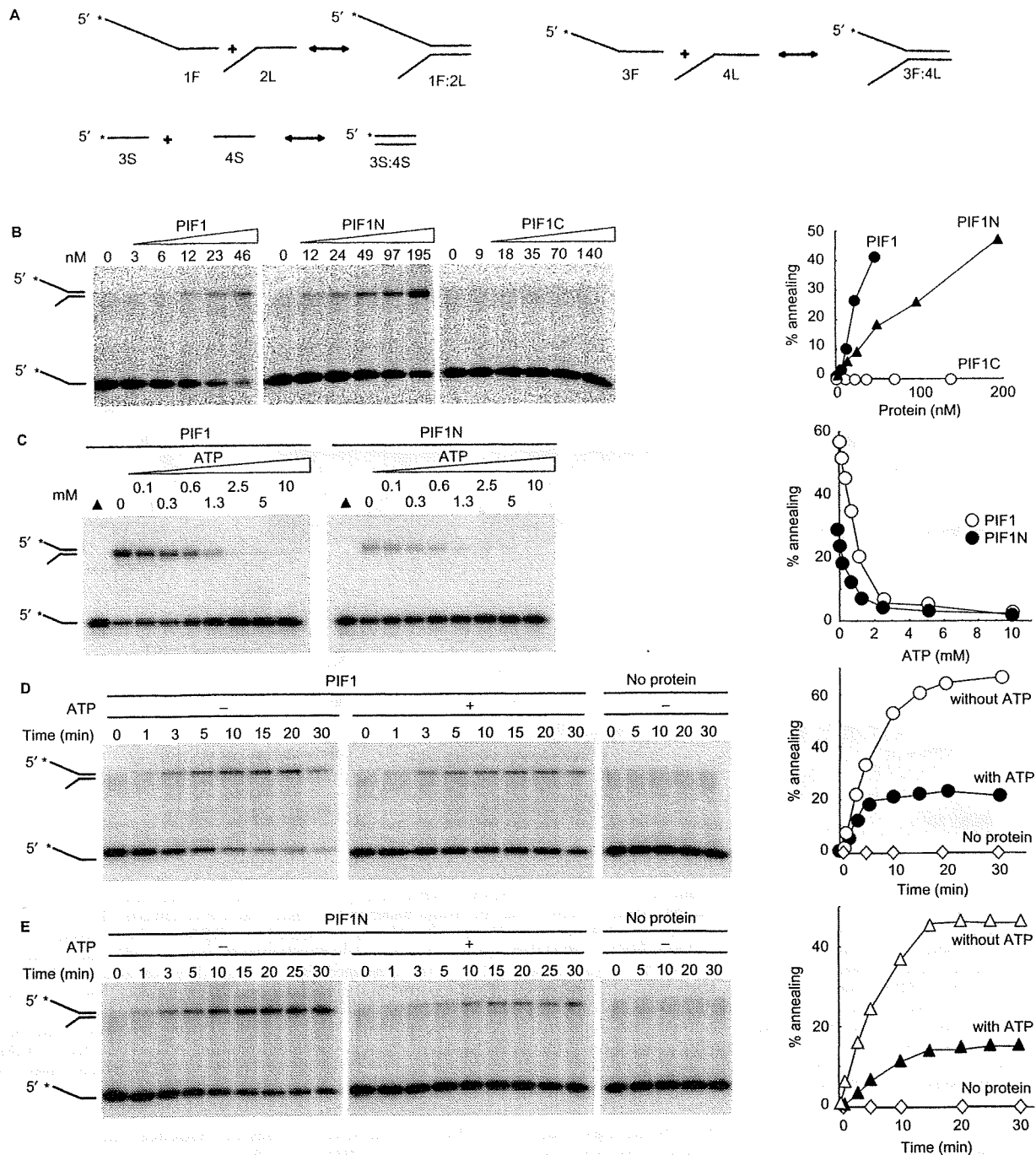
Figure 5. DNA strand annealing activity. (A) Schematic structures of the DNA substrates. The asterisks indicate ^{32}P-labeled 5′-phosphate. (B) Annealing activities of PIF1, PIF1C and PIF1N. The fork-structural partial duplex DNA substrate, 1F:2L (0.35 nM), was boiled for 5 min, then incubated with increasing levels of PIF1, PIF1C and PIF1N as indicated under standard reaction conditions omitting ATP at 30°C for 10 min. The quantified data are shown graphically. (C) Titration of ATP on annealing reactions mediated by PIF1 and PIF1N. The fork-structural partial duplex DNA substrate, 3F:4L (0.35 nM), was boiled for 5 min, then incubated with PIF1 (33 nM) or PIF1N (195 nM) and increasing levels of ATP under standard reaction conditions omitting MgCl$_2$ at 30°C for 10 min. The quantified data are shown graphically. (D) Time course of annealing reactions mediated by PIF1 under standard reaction conditions omitting MgCl$_2$. Heat denatured substrate DNA, 1F:2L (0.35 nM), was incubated with PIF1 (46 nM). The quantified data are shown graphically. (E) Time course of annealing reactions mediated by PIF1N under standard reaction conditions omitting MgCl$_2$. Heat denatured substrate DNA, 1F:2L (0.35 nM), was incubated with PIF1N (195 nM). The quantified data are shown graphically. (F) Titration of ATP on annealing reactions mediated by PIF1 and PIF1N under standard reaction conditions. A complete double stranded oligonucleotide, 3S:4S (0.35 nM) was boiled for 5 min, then incubated with PIF1 (30 nM) or PIF1N (195 nM) and increasing levels of ATP under standard reaction conditions at 30°C for 10 min. The quantified data are shown graphically. The errors in the experiments were <10%.
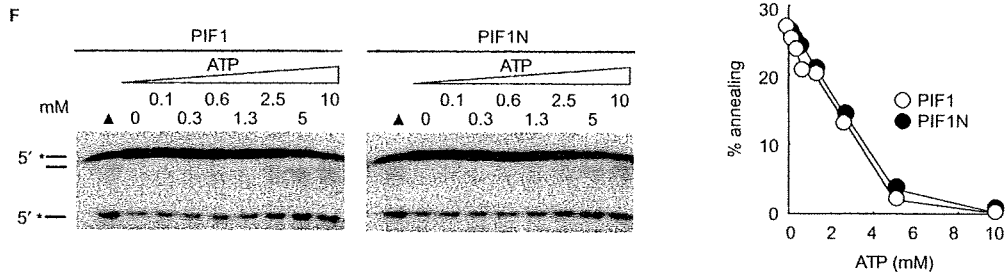
Figure 5. Continued.
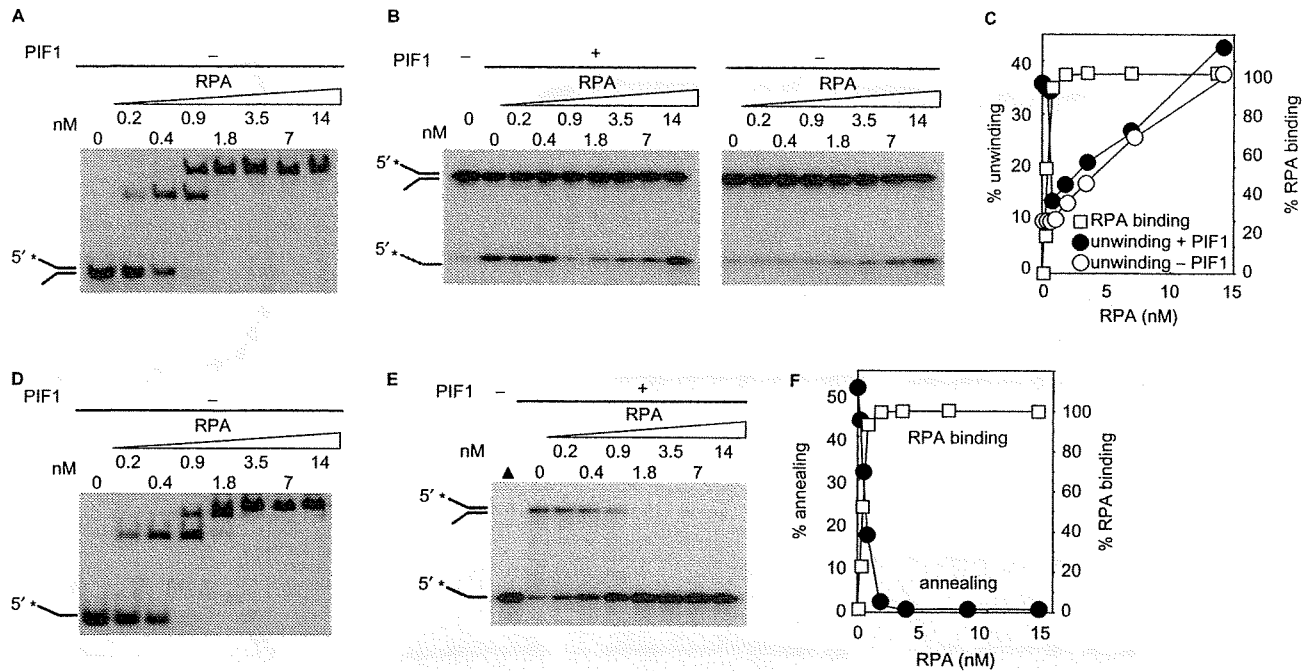
Figure 6. Effects of RPA on the unwinding and annealing reactions. (A) EMSA of RPA binding. The fork-structural partial duplex DNA substrate, 3F:4L (0.35 nM) was incubated with RPA at indicated concentrations on ice for 10 min under the standard reaction conditions. (B) Unwinding assay in the presence of RPA. The fork-structural partial duplex DNA substrate, 3F:4L (0.35 nM), was incubated with RPA at indicated concentrations on ice for 10 min under standard reaction conditions. Then, PIF1 (16 nM) (left panel) and buffer (right panel) were introduced and incubated at 30°C for 10 min. Reaction products were separated on a 15–25% polyacrylamide gel. (C) The quantified data of unwinding reactions in (B) are shown graphically with the RPA binding curve in (A). (D) EMSA of RPA binding. The fork-structural partial duplex DNA substrate, 3F:4L (0.35 nM), was boiled for 5 min, then incubated with RPA at indicated concentrations on ice for 10 min under the standard reaction conditions omitting ATP. (E) Annealing assay in the presence of RPA. The fork-structural partial duplex DNA substrate, 3F:4L (0.35 nM) (Figure 5A), was boiled for 5 min, then incubated with RPA at indicated concentrations on ice for 10 min under standard reaction conditions omitting ATP. Then PIF1 (30 nM) was introduced and incubated at 30°C for 10 min. Reaction products were separated on a 15–25% polyacrylamide gel. (F) The quantified data of annealing reactions in (E) are shown graphically with the RPA binding curve in (D). The errors in the experiments were <10%.

Biochemical analysis of yeast PIF1 homologs has demonstrated that they preferentially unwind forked substrates (1,5,7). We showed that the property is conserved in human PIF1. However, we found that forked substrates were not optimal with respect to stimulation of ATPase activity. Rather nonstructural ssDNA greatly stimulated ATPase activity. The finding that the K_{eff} value for nonstructural ssDNA was lower than for other DNA molecules, including forked structures, suggested preferential binding of PIF1 to ssDNA. From these results, we suggest that PIF1 needs an ssDNA region for loading and a forked structure for entrance to the double strand region by translocation.

We present several lines of evidence that the enzymatic characters of PIF1C reflect the intrinsic properties of the helicase domain. First, PIF1C expressed ATPase activity to the level equivalent to full-length PIF1 (about 1000 min^{-1}) and also equivalent to that for yeast homologs (5,7). Second, full-length PIF1 and PIF1C both showed a similar preference for poly(purine–pyrimidine) and polypyrimidine, but not polypurine, for stimulation of ATPase. This property is also conserved in yeast homologs (5,7). Third, the K_m values for ATP of full-length PIF1 and PIF1C were essentially identical. This is also in agreement with a previous report for N-terminal truncated PIF1, purified as a C-terminus GST-fusion protein (4).

These results suggest that the determined properties of PIF1C are intrinsic to the helicase domain, and could also exclude the possibility that the his-tag at the N-terminal of PIF1C interferes with activities of the helicase domain.

Interestingly, we noted a significant difference between PIF1 and PIF1C with regard to the required concentration of ssDNA for stimulation of ATPase activity. PIF1C needed a 20 times higher concentration and also exhibited much lower unwinding activity. The results suggest that the defects could be attributed to missing functions of the PINT domain. The difference in the K_{eff} values could be due to lower binding affinity of the helicase domain for ssDNA. Consequently, we demonstrated ssDNA binding of PIF1 directly by EMSA. The apparent K_d value, 3 nM was in good agreement with the K_{eff} value of 2 nM when expressed with reference to the oligonucleotide concentration, suggesting that this assay well reflected the functional interaction between ssDNA and PIF1. In this assay, as expected, we demonstrated lower affinity of PIF1C to ssDNA. We suggested that the defect in PIF1C could be due, at least in part, to lower binding affinity for ssDNA, and the PINT domain plays a role for increasing this affinity of the helicase domain. Notably, the K_d value (10 nM) of PIF1C determined by EMSA was still 6 times lower than the K_{eff} value (60 nM in oligonucleotides) for the ATPase assay. We consider the following possible explanations for the discrepancy. We found that PIF1C exhibited a much higher affinity for ssDNA without binding of ATP. With the EMSA, an ATP-free fraction of PIF1C could exist, even in the presence of ATP. Therefore, the results could be an overestimation, due to high affinity binding of the ATP-free fraction of PIF1C. Alternatively, the PINT domain could possess another function for enhancing activity of the helicase domain by modulating the mode of interaction with ssDNA. The higher affinity of PIF1C for ssDNA without binding of ATP could be intrinsic to the helicase domain. The results suggested that ATP modulated the binding mode with ssDNA. The higher affinity to ssDNA before binding of ATP is reduced by binding of ATP. The alteration must be alternatively repeated during turnover of reactions of ATPase. With the full-length PIF1, such alteration due to ATP binding was not detected, suggesting that the PINT domain somehow could suppress the alteration during turnover of ATPase reactions. In this study, we demonstrated that the PINT domain also possesses ssDNA binding activity. We suggest that its enhancement of the activities of the helicase domain is due, at least in part, to this ssDNA binding activity.

We unexpectedly found the PINT domain to further possess ssDNA annealing activity. Among the proteins handled in this study having ssDNA binding activity, including PIF1C, PIF1N and RPA, we could detect annealing activity only with PIF1N. We consider that the annealing activity could be mediated by ssDNA binding, although not attributable to the general effect of high affinity ssDNA binding. Annealing activity has been reported to be associated with the RecQ family helicase in general (39–45). While the RecQ family is distinct from PIF1 family, annealing activity shares similar properties

in common. It is located outside of the conserved helicase domains (39,40), is inhibited by RPA, and is ATP-independent or rather inhibited by ATP (39–42,44). We demonstrated that inhibition by ATP is not a consequence of the unwinding reaction, suggesting that it is an intrinsic property of the PINT domain.

At the present time, the biological significance of our findings cannot be readily assessed. Importantly, we showed that RPA inhibited unwinding and annealing reactions, suggesting that these functions of PIF1 might be restricted under particular situations in DNA metabolism. There is a marked difference from RecQ helicases, whose unwinding activity is proficient on RPA-coated ssDNA and stimulated by RPA, although annealing activity is suppressed (39–41,46–48). Notably, unwinding activity of *Sc*Pif1 was stimulated by RPA (1), but that of the fission yeast homolog, Pfh1, was inhibited (7) like human PIF1, suggesting that the outcomes in cells would differ. This could be related to the fact that budding yeast has another member of the PIF1 superfamily, Rrm3, but human and fission yeast have only one. Further analysis of the precise cellular roles of PIF1 should shed light on functions in maintenance of genetic stability.

SUPPLEMENTARY DATA

Supplementary Data are available at NAR Online.

REFERENCES

1. Boulé,J.B. and Zakian,V.A. (2007) The yeast Pif1p DNA helicase preferentially unwinds RNA DNA substrates. *Nucleic Acids Res.*, **35**, 5809–5818.

2. Foury,F. and Lahaye,A. (1987) Cloning and sequencing of the *PIF* gene involved in repair and recombination of yeast mitochondrial DNA. *EMBO J.*, **6**, 1441–1449.

3. Futami,K., Shimamoto,A. and Furuichi,Y. (2007) Mitochondrial and nuclear localization of human Pif1 helicase. *Biol. Pharm. Bull.*, **30**, 1685–1692.

4. Huang,Y., Zhang,D.H. and Zhou,J.Q. (2006) Characterization of ATPase activity of recombinant human Pif1. *Acta. Biochim. Biophys. Sin. (Shanghai).*, **38**, 335–341.

5. Lahaye,A., Leterme,S. and Foury,F. (1993) PIF1 DNA helicase from *Saccharomyces cerevisiae*. Biochemical characterization of the enzyme. *J. Biol. Chem.*, **268**, 26155–26161.

6. Lahaye,A., Stahl,H., Thines-Sempoux,D. and Foury,F. (1991) PIF1: a DNA helicase in yeast mitochondria. *EMBO J.*, **10**, 997–1007.

7. Ryu,G.H., Tanaka,H., Kim,D.H., Kim,J.H., Bae,S.H., Kwon,Y.N., Rhee,J.S., MacNeill,S.A. and Seo,Y.S. (2004) Genetic and biochemical analyses of Pfh1 DNA helicase function in fission yeast. *Nucleic Acids Res.*, **32**, 4205–4216.

8. Tanaka,H., Ryu,G.H., Seo,Y.S., Tanaka,K., Okayama,H., MacNeill,S.A. and Yuasa,Y. (2002) The fission yeast *pfh1+* gene encodes an essential 5′ to 3′ DNA helicase required for the completion of S-phase. *Nucleic Acids Res.*, **30**, 4728–4739.

9. Zhang,D.H., Zhou,B., Huang,Y., Xu,L.X. and Zhou,J.Q. (2006) The human Pif1 helicase, a potential *Escherichia coli* RecD homologue, inhibits telomerase activity. *Nucleic Acids Res.*, **34**, 1393–1404.

10. Zhou,J.Q., Qi,H., Schulz,V.P., Mateyak,M.K., Monson,E.K. and Zakian,V.A. (2002) *Schizosaccharomyces pombe pfh1+* encodes an essential 5′ to 3′ DNA helicase that is a member of the PIF1 subfamily of DNA helicases. *Mol. Biol. Cell*, **13**, 2180–2191.

11. Bessler,J.B., Torredagger,J.Z. and Zakian,V.A. (2001) The Pif1p subfamily of helicases: region-specific DNA helicases? *Trends Cell Biol.*, **11**, 60–65.

12. Foury,F. and Dyck,E.V. (1985) A PIF-dependent recombinogenic signal in the mitochondrial DNA of yeast. *EMBO J.*, **4**, 3525–3530.

13. Foury,F. and Kolodynski,J. (1983) *pif* mutation blocks recombination between mitochondrial ρ⁺ and ρ⁻ genomes having tandemly arrayed repeat units in *Saccharomyces cerevisiae*. *Proc. Natl Acad. Sci. USA*, **80**, 5345–5349.

14. Doudican,N.A., Song,B., Shadel,G.S. and Doetsch,P.W. (2005) Oxidative DNA damage causes mitochondrial genomic instability in *Saccharomyces cerevisiae*. *Mol. Cell Biol.*, **25**, 5196–5204.

15. O'Rourke,T.W., Doudican,N.A., Mackereth,M.D., Doetsch,P.W. and Shadel,G.S. (2002) Mitochondrial dysfunction due to oxidative mitochondrial DNA damage is reduced through cooperative actions of diverse proteins. *Mol. Cell Biol.*, **22**, 4086–4093.

16. O'Rourke,T.W., Doudican,N.A., Zhang,H., Eaton,J.S., Doetsch,P.W. and Shadel,G.S. (2005) Differential involvement of the related DNA helicases Pif1p and Rrm3p in mtDNA point mutagenesis and stability. *Gene*, **354**, 86–92.

17. Cheng,X., Dunaway,S. and Ivessa,A.S. (2007) The role of Pif1p, a DNA helicase in *Saccharomyces cerevisiae*, in maintaining mitochondrial DNA. *Mitochondrion*, **7**, 211–222.

18. Zhou,J., Monson,E.K., Teng,S.C., Schulz,V.P. and Zakian,V.A. (2000) Pif1p helicase, a catalytic inhibitor of telomerase in yeast. *Science*, **289**, 771–774.

19. Schulz,V.P. and Zakian,V.A. (1994) The *Saccharomyces PIF1* DNA helicase inhibits telomere elongation and *de novo* telomere formation. *Cell*, **76**, 145–155.

20. Kanaar,R., Wyman,C. and Rothstein,R. (2008) Quality control of DNA break metabolism: in the 'end', it's a good thing. *EMBO J.*, **27**, 581–588.

21. Mangahas,J.L., Alexander,M.K., Sandell,L.L. and Zakian,V.A. (2001) Repair of chromosome ends after telomere loss in *Saccharomyces*. *Mol. Biol. Cell*, **12**, 4078–4089.

22. Mateyak,M.K. and Zakian,V.A. (2006) Human PIF helicase is cell cycle regulated and associates with telomerase. *Cell Cycle*, **5**, 2796–2804.

23. Myung,K., Chen,C. and Kolodner,R.D. (2001) Multiple pathways cooperate in the suppression of genome instability in *Saccharomyces cerevisiae*. *Nature*, **411**, 1073–1076.

24. Pennaneach,V., Putnam,C.D. and Kolodner,R.D. (2006) Chromosome healing by de novo telomere addition in *Saccharomyces cerevisiae*. *Mol. Microbiol.*, **59**, 1357–1368.

25. Boulé,J.B., Vega,L.R. and Zakian,V.A. (2005) The yeast Pif1p helicase removes telomerase from telomeric DNA. *Nature*, **438**, 57–61.

26. Budd,M.E., Reis,C.C., Smith,S., Myung,K. and Campbell,J.L. (2006) Evidence suggesting that Pif1 helicase functions in DNA replication with the Dna2 helicase/nuclease and DNA polymerase δ. *Mol. Cell Biol.*, **26**, 2490–2500.

27. Ivessa,A.S., Zhou,J.Q. and Zakian,V.A. (2000) The *Saccharomyces* Pif1p DNA helicase and the highly related Rrm3p have opposite effects on replication fork progression in ribosomal DNA. *Cell*, **100**, 479–489.

28. Wagner,M., Price,G. and Rothstein,R. (2006) The absence of Top3 reveals an interaction between the Sgs1 and Pif1 DNA helicases in *Saccharomyces cerevisiae*. *Genetics*, **174**, 555–573.

29. Masuda,Y., Suzuki,M., Piao,J., Gu,Y., Tsurimoto,T. and Kamiya,K. (2007) Dynamics of human replication factors in the elongation phase of DNA replication. *Nucleic Acids Res.*, **35**, 6904–6916.

30. Henricksen,L.A., Umbricht,C.B. and Wold,M.S. (1994) Recombinant replication protein A: expression, complex formation, and functional characterization. *J. Biol. Chem.*, **269**, 11121–11132.

31. Studier,F.W., Rosenberg,A.H., Dunn,J.J. and Dubendorff,J.W. (1990) Use of T7 RNA polymerase to direct expression of cloned genes. *Methods Enzymol.*, **185**, 60–89.

32. Snaith,M.R., Kilby,N.J. and Murray,J.A. (1996) An *Escherichia coli* system for assay of Flp site-specific recombination on substrate plasmids. *Gene*, **180**, 225–227.

33. Sambrook,J., Fritsch,E.F. and Maniatis,T. (1989) *Molecular Cloning: A Laboratory Manual*, 2nd ed. Cold Spring Harbor Laboratory Press, Cold Spring Harbor, NY.

34. Masuda,Y., Takahashi,M., Tsunekuni,N., Minami,T., Sumii,M., Miyagawa,K. and Kamiya,K. (2001) Deoxycytidyl transferase activity of the human REV1 protein is closely associated with the conserved polymerase domain. *J. Biol. Chem.*, **276**, 15051–15058.

35. Carey,J. (1991) Gel retardation. *Methods Enzymol.*, **208**, 103–117.

36. Kornberg,A., Scott,J.F. and Bertsch,L.L. (1978) ATP utilization by rep protein in the catalytic separation of DNA strands at a replicating fork. *J. Biol. Chem.*, **253**, 3298–3304.

37. Matson,S.W. and George,J.W. (1987) DNA helicase II of *Escherichia coli*. Characterization of the single-stranded DNA-dependent NTPase and helicase activities. *J. Biol. Chem.*, **262**, 2066–2076.

38. Wold,M.S. (1997) Replication protein A: a heterotrimeric, single-stranded DNA-binding protein required for eukaryotic DNA metabolism. *Annu. Rev. Biochem.*, **66**, 61–92.

39. Cheok,C.F., Wu,L., Garcia,P.L., Janscak,P. and Hickson,I.D. (2005) The Bloom's syndrome helicase promotes the annealing of complementary single-stranded DNA. *Nucleic Acids Res.*, **33**, 3932–3941.

40. Garcia,P.L., Liu,Y., Jiricny,J., West,S.C. and Janscak,P. (2004) Human RECQ5β, a protein with DNA helicase and strand-annealing activities in a single polypeptide. *EMBO J.*, **23**, 2882–2891.

41. Kanagaraj,R., Saydam,N., Garcia,P.L., Zheng,L. and Janscak,P. (2006) Human RECQ5β helicase promotes strand exchange on synthetic DNA structures resembling a stalled replication fork. *Nucleic Acids Res.*, **34**, 5217–5231.

42. Machwe,A., Xiao,L., Groden,J., Matson,S.W. and Orren,D.K. (2005) RecQ family members combine strand pairing and unwinding activities to catalyze strand exchange. *J. Biol. Chem.*, **280**, 23397–23407.

43. Macris,M.A., Krejci,L., Bussen,W., Shimamoto,A. and Sung,P. (2006) Biochemical characterization of the RECQ4 protein, mutated in Rothmund-Thomson syndrome. *DNA Repair (Amst).*, **5**, 172–180.

44. Sharma,S., Sommers,J.A., Choudhary,S., Faulkner,J.K., Cui,S., Andreoli,L., Muzzolini,L., Vindigni,A. and Brosh,R.M. Jr (2005) Biochemical analysis of the DNA unwinding and strand annealing activities catalyzed by human RECQ1. *J. Biol. Chem.*, **280**, 28072–28084.

45. Machwe,A., Lozada,E.M., Xiao,L. and Orren,D.K. (2006) Competition between the DNA unwinding and strand pairing activities of the Werner and Bloom syndrome proteins. *BMC Mol. Biol.*, **7**, 1.

46. Brosh,R.M. Jr, Orren,D.K., Nehlin,J.O., Ravn,P.H., Kenny,M.K., Machwe,A. and Bohr,V.A. (1999) Functional and physical interaction between WRN helicase and human replication protein A. *J. Biol. Chem.*, **274**, 18341–18350.

47. Brosh,R.M. Jr, Li,J.L., Kenny,M.K., Karow,J.K., Cooper,M.P., Kureekattil,R.P., Hickson,I.D. and Bohr,V.A. (2000) Replication protein A physically interacts with the Bloom's syndrome protein and stimulates its helicase activity. *J. Biol. Chem.*, **275**, 23500–23508.

48. Cui,S., Arosio,D., Doherty,K.M., Brosh,R.M. Jr, Falaschi,A. and Vindigni,A. (2004) Analysis of the unwinding activity of the dimeric RECQ1 helicase in the presence of human replication protein A. *Nucleic Acids Res.*, **32**, 2158–2170.

Absence of *Ku70* Gene Obliterates X-Ray-Induced *lacZ* Mutagenesis of Small Deletions in Mouse Tissues

Yoshihiko Uehara,[a] Hironobu Ikehata,[a] Jun-ichro Komura,[a] Ari Ito,[a] Masaki Ogata,[a] Tsunetoshi Itoh,[a]
Ryoichi Hirayama,[b] Yoshiya Furusawa,[b] Koichi Ando,[b] Tatjana Paunesku,[c] Gayle E. Woloschak,[c] Kenshi Komatsu,[d]
Shinya Matsuura,[e] Tsuyoshi Ikura,[a] Kenji Kamiya[e] and Tetsuya Ono[a,1]

[a] *Department of Cell Biology, Graduate School of Medicine, Tohoku University, 2-1 Seiryo-machi, Aoba-ku, Sendai 980-8575, Japan;* [b] *Heavy-Ion
Radiobiology Research Group, National Institute of Radiological Sciences, Anagawa 4-9-1, Inage-ku, Chiba 263-8555, Japan;*
[c] *Department of Radiology, Feinberg School of Medicine, Northwestern University, Chicago, IL 60611;* [d] *Department of Genome Repair Dynamics,
Radiation Biology Center, Kyoto University, Yoshida-konoe, Sakyo-ku, Kyoto 606-8501, Japan; and* [e] *Research Institute for Radiation Biology and
Medicine, Hiroshima University, Kasumi-ku, Hiroshima 734-8553, Japan*

Uehara, Y., Ikehata, H., Komura, J-I., Ito, A., Ogata, M.,
Itoh, T., Hirayama, R., Furusawa, Y., Ando, K., Paunesku, T.,
Woloschak, G. E., Komatsu, K., Matsuura, S., Ikura, T., Ka-
miya, K. and Ono, T. Absence of *Ku70* Gene Obliterates X-
Ray-Induced *lacZ* Mutagenesis of Small Deletions in Mouse
Tissues. *Radiat. Res.* 170, 216–223 (2008).

With the goal of understanding the role of non-homologous
end-joining repair in the maintenance of genetic information
at the tissue level, we studied mutations induced by radiation
and subsequent repair of DNA double-strand breaks in *Ku70*
gene-deficient *lacZ* transgenic mice. The local mutation fre-
quencies and types of mutations were analyzed on a *lacZ* gene
that had been chromosomally integrated, which allowed us to
monitor DNA sequence alterations within this 3.1-kbp region.
The mutagenic process leading to the development of the most
frequently observed small deletions in wild-type mice after
exposure to 20 Gy of X rays was suppressed in $Ku70^{-/-}$ mice
in the three tissues examined: spleen, liver and brain. Exam-
ination of DNA break rejoining and the phosphorylation of
histone H2AX in *Ku70*-deficient and -proficient mice revealed
that *Ku70* deficiency decreased the frequency of DNA rejoin-
ing, suggesting that DNA rejoining is one of the causes of
radiation-induced deletion mutations. Limited but statistically
significant DNA rejoining was found in the liver and brain of
Ku70-deficient mice 3.5 days after irradiation, showing the
presence of a DNA double-strand break repair system other
than non-homologous end joining. These data indicate a pre-
dominant role of non-homologous end joining in the produc-
tion of radiation-induced mutations *in vivo*. © 2008 by Radiation
Research Society

INTRODUCTION

DNA double-strand breaks cause serious problems for
cells because their presence leads to losses of small and

[1] Address for correspondence: Department of Cell Biology, Graduate
School of Medicine, Tohoku University, 2-1 Seiryo-machi, Aoba-ku, Sen-
dai 980-8575, Japan; e-mail: tono@mail.tains.tohoku.ac.jp.

large DNA fragments. Two kinds of DNA repair systems
are known to work to rejoin these breaks: non-homologous
end joining (NHEJ) and homologous recombination repair
(HRR). In many higher organisms, NHEJ has been shown
to play a major role in genome maintenance. NHEJ occurs
through the collaboration of several proteins, including
Ku70, Ku80, DNA-PKcs, ligase IV and Cernunnos-XLF
(*1–6*). Inactivation of the NHEJ system by knocking out
one of the key genes in this repair pathway results in severe
health problems including immunodeficiency, developmen-
tal abnormalities, early cancer development, and premature
aging. Among these, cancer and premature aging are as-
sumed to be induced at least in part by genomic instability
caused by the lack of repair of spontaneously occurring
DNA double-strand breaks (*1–4, 7, 8*). However, this as-
sumption is not clearly established. Genomic alterations in-
duced by DNA double-strand breaks are grouped into two
categories: (1) large-scale changes such as chromosomal
fragmentation, rearrangement of large DNA fragments, and
telomere defects; (2) alteration of DNA at the gene se-
quence level, resulting in gene mutations. Studies on chro-
mosomal structures in untreated NHEJ-deficient cultured
cells showed elevated levels of fragmented and translocated
chromosomes (*9–11*). Untreated NHEJ-deficient mice with
an inactivated *Ku80* gene, on the other hand, had a reduced
level of spontaneous large-scale DNA rearrangements com-
pared to wild-type mice as judged by a chromosomally in-
tegrated *lacZ* gene enclosed in plasmid DNA (*12*). The dis-
crepancy could be explained by elimination of cells con-
taining chromosomal rearrangements *in vivo* by apoptosis,
although little evidence is available to support this. Irradi-
ation of cultured cells induces chromosomal abnormalities,
which become even more frequent in NHEJ-deficient cells
(*13*). This finding was supported by biochemical analyses
of DNA rejoining using pulsed-field gel electrophoresis
combined with Southern blot analysis (*14*). NHEJ deficien-
cy resulted in the suppression of rejoining of 50% of the

216

radiation-induced DNA double-strand breaks—a finding that is in agreement with elevated chromosomal fragment formation in irradiated NHEJ-deficient cells (*13*). Interestingly, the remaining 50% of the breaks were rejoined correctly in both wild-type and NHEJ-deficient cells, indicating the presence of an error-free repair system working independently from NHEJ. The method, however, identifies DNA of Mbp sizes and does not detect DNA alterations of less than a few hundred kbp. Thus the correct rejoining in the context of these published studies does not reflect the degree of DNA sequence maintenance at the nucleotide level such as base substitutions and short-fragment DNA deletions and insertions. More detailed studies were done with mutation analysis. However, the mutation studies performed on the cultured cells for the effect of NHEJ deficiency were complicated. The spontaneous mutation levels of both the *TK* and *HPRT* genes were not affected by DNA-PKcs deficiency, and radiation-induced mutation was suppressed at the *TK* locus but not at the *HPRT* locus (*15*). Ku-deficient Chinese hamster cells were shown to be sensitive to mutation induction at the *HPRT* locus using bleomycin, a drug that induces DNA double-strand breaks (*16*). In vivo studies of the role of NHEJ for radiation-induced mutation of single genes have not been performed previously.

Previously, we studied the molecular nature of mutations induced by radiation in mouse tissues using a chromosomally integrated *lacZ* gene enclosed in lambda DNA as a marker, and we found that the predominant type of mutation was deletion of one to a few hundred base pairs (*17*). Similar results were observed subsequently in a gpt delta transgenic mouse (*18*). This type of mutation is shown to be produced through errors associated with NHEJ repair of DNA double-strand breaks that were created either in the process of DNA rearrangement of antigen-receptor genes (*19*) or by restriction enzyme-induced double-strand breaks (*20–22*). Therefore, we postulated that NHEJ could be responsible for the major type of mutation found in tissues as a consequence of radiation exposure. We analyzed mutant frequencies and the molecular nature of the mutants as well as rejoining of DNA breaks in *Ku70*-knockout *lacZ* transgenic mice. Since the genome maintenance system in each tissue is unique and DNA repair and the mutational burden vary among different tissues (*23–27*), we examined three tissues with different cell renewal properties: spleen, liver and brain.

MATERIALS AND METHODS

Mice

Muta® mice, which harbor the *lacZ*-containing lambda phage genome as a transgene (*28*), were purchased from Covance Research Products, Denver, PA. The genetic background of the mice was a mixture of BALB/c and DBA/2 (*28*). The Muta® mice were mated with *Ku70*⁺/⁻ mice (*29*). F₁ mice of the *Ku70*⁺/⁻, *lacZ*⁺ genotype were selected and mated again to obtain *Ku70*⁻/⁻, *lacZ*⁺; *Ku70*⁺/⁻, *lacZ*⁺; and *Ku70*⁺/⁺, *lacZ*⁺ mice. The genotype of *Ku70* was determined by PCR as described previously (*29*).

The PCR primers for *lacZ* were 5'-(-84)CACCCCAGGCTTTACACT TT (sense primer) and 5'-(2525)ATCAGCACCGCATCAGCAAG (antisense primer). The PCR conditions were 94°C for 4 min followed by 28 cycles of 94°C for 30 s, 55°C for 1 min and 72°C for 1 min and a final incubation at 72°C for 4 min (*30*).

Irradiation

Two-month-old mice were placed in a plastic box in which they could move freely and were irradiated with 20 or 50 Gy of X rays (200 kVp, 10 mA, filtered with 1 mm aluminum and 0.5 mm copper, 0.72 Gy/min, Shimadzu HF320, Kyoto, Japan). For the analysis of DNA fragmentation, mice were irradiated at a higher dose rate to minimize DNA rejoining during irradiation (220 kVp, 17 mA, filtered with 0.5 mm aluminum and 0.3 mm copper, 5.83 Gy/min). The tissues were harvested immediately (2 to 3 min), 1 h or 3.5 days after irradiation. The animal experiments were conducted according to the Guidelines for Animal Welfare and Experimentation at Tohoku University.

Mutation Assay

Mutant frequencies were determined at 3.5 days after irradiation. Genomic DNA was isolated from tissues by phenol extraction and mixed with lambda phage packaging extract (Transpack® Packaging Extract, Stratagene, La Jolla, CA). The number of phages retrieved containing the *lacZ* gene was estimated by the number of plaques that developed on *E. coli* strain C of galE⁻. The number of phages containing a mutated *lacZ* gene was counted as plaques observed in the presence of phenyl-β-D-galactose. Two or three *Ku70*⁺/⁺ and *Ku70*⁺/⁻ mice and three or four *Ku70*⁻/⁻ mice were examined.

Sequencing of the mutant *lacZ* gene was done by a DNA sequencer (ABI PRISM® 3100, Applied Biosystems, Foster City, CA), and the sequences obtained were compared to the nucleotide sequence of the wild-type *lacZ* gene. For the analysis of the mutation spectrum, two or more mutants showing identical characteristics to the other mutant found in the same DNA preparation were eliminated from counting to avoid a possible effect of replication of mutation. The details of this procedure were described previously (*24, 30*).

SFGE Analysis of DNA Breaks

To monitor DNA breaks and rejoining, static-field gel electrophoresis (SFGE) was used (*31*). A part of the spleen or liver or a longitudinal half of a brain was minced with a pair of scissors, dissolved in phosphate-buffered saline, pipetted about 10 times to disassociate cells, strained through a 40-μm mesh strainer (BD Falcon, Bedford, MA), and rinsed twice by centrifugation. The spleen cell density was adjusted to 2.5 × 10⁷ cells/ml. The liver and brain cell suspensions were adjusted to OD₆₀₀ = 12 using a spectrophotometer, because the cells were difficult to count. The cell suspension (15 μl) was embedded in 55 μl of 1.3% agarose and lysed with lysis buffer and proteinase K at 50°C, 24 h (CHEF Genomic DNA Plug Kits, Bio-Rad Laboratories, Hercules, CA). The DNA was electrophoresed for 36 h at 0.6 V/cm. The DNA remaining in the well and the DNA released into the gel were quantified after staining with ethidium bromide. The details of this procedure were described previously (*31*). The fraction of DNA released from the wells was used as a measure of DNA breaks.

Western Blot Analysis of γ-H2AX

Approximately 0.1 g of spleen or 0.3 g of liver was minced with a pair of scissors and homogenized in a glass homogenizer in lysis buffer containing 0.5% Triton X-100. For brain, a longitudinal half of a whole organ was used. The homogenized samples were centrifuged at 800g for 2 min, and the precipitated nuclei were rinsed again with lysis buffer. The nuclei were lysed with 1% of SDS, and the DNA was fragmented by sonication. After the insoluble material was pelleted, nuclear proteins were separated by 15% SDS-polyacrylamide gel electrophoresis, trans-
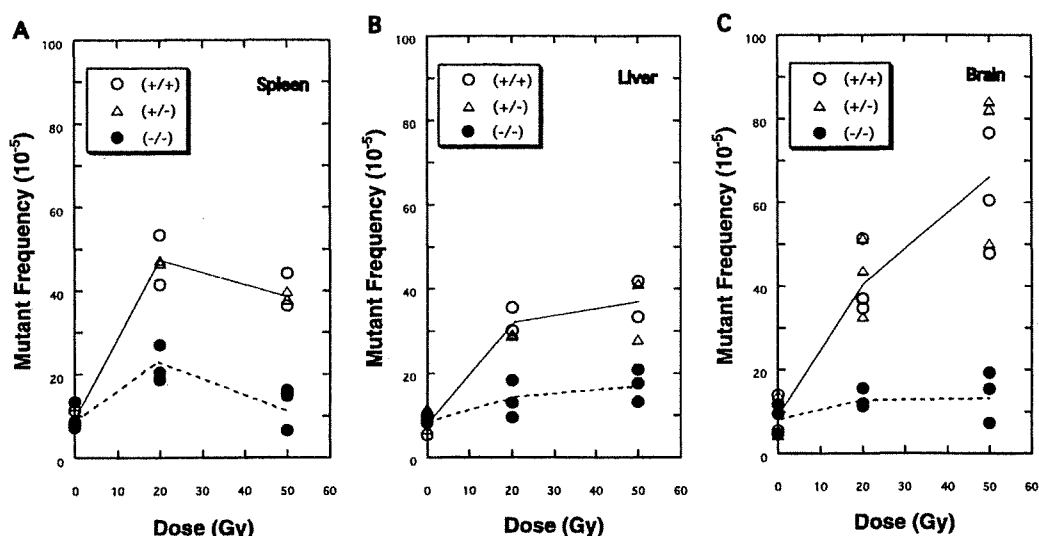
FIG. 1. Effects of *Ku70* genotype on radiation-induced *lacZ* mutations in the spleen (panel A), liver (panel B) and brain (panel C) of Muta® mouse. Mutant frequencies after whole-body exposure to 0, 20 and 50 Gy radiation were examined in *Ku70*⁺/⁺, ⁺/⁻ and ⁻/⁻ *lacZ* transgenic mice. No difference was observed between *Ku70*⁺/⁺ and ⁺/⁻ mice.

ferred to nitrocellulose membranes, and analyzed for H2AX and phosphorylated H2AX (γ-H2AX) using antibodies specific for each protein; anti-H2AX Ab was made using the C terminal peptide of human H2AX as an antigen; a monoclonal Ab for γ-H2AX [Phospho-Histone H2AX (Ser139)] was purchased from Cell Signaling Technology Inc., Danvers, MA). The procedures have been described elsewhere (*32*). Non-phosphorylated and phosphorylated H2AX were compared by Western blots as an indication of the presence of DNA breaks in cells (*33*).

RESULTS

Radiation-Induced Mutations

The mutant frequencies in spleen, liver and brain after exposure to 0, 20 or 50 Gy X rays are shown in Fig. 1. *Ku70*⁺/⁺ and ⁺/⁻ mice showed increased mutation frequencies after irradiation, whereas *Ku70*⁻/⁻ mice showed reduced mutation levels in all three tissues compared to *Ku70*-proficient mice. *Ku70*⁺/⁺ and ⁺/⁻ mice had no appreciable differences. The spontaneous levels of mutations were similar for all three genotypes. The number of mutations induced by 20 Gy were calculated by subtracting the average mutant frequency of nonirradiated mice from that of irradiated mice. The numbers of induced mutations in *Ku70*-proficient and -deficient mice were compared to determine the percentages of mutations produced through a *Ku70*-dependent NHEJ process; they were 67, 82 and 86% in spleen, liver and brain, respectively.

To understand the molecular mechanisms underlying these differences, we sequenced the *lacZ* DNA of the mutant clones. The frequencies of the different types of mutations are shown in Fig. 2. In *Ku70*⁺/⁺ and ⁺/⁻ mice, the predominant type of mutation induced by radiation was a deletion, whereas this type of mutation was much less frequent in *Ku70*⁻/⁻ mice. The results were similar in all three

tissues we examined. This indicates that the predominant type of mutation induced by radiation at the gene sequence level, a deletion, is produced through a *Ku70*-dependent NHEJ process.

Recently, Honma *et al.* reported that the predominant mutations produced at double-strand break sites made by restriction enzyme I-*Sce*I were 1- to 50-bp-long deletions (*22*). Hence we classified the deletion mutations we found into two groups: 1–50 bp and more than 50 bp (Table 1). All of the spontaneous mutations were in the former group, whereas radiation induced deletion mutations of both sizes. In *Ku70*-proficient irradiated mice, 1–50 bp was predominant, but this was not the case in *Ku70*-deficient irradiated mice (Table 1). In other words, *Ku70* deficiency results in the suppression of small deletions of 1 to 50 bp rather than the larger deletions.

Details about the infrequent mutations classified as multiple and complex mutations in Fig. 2 are presented in Table 2. These types of mutations are observed only in irradiated mice, with the exception of one found in the unirradiated spleen of the *Ku70*⁻/⁻ mouse. The complex-type mutations can be explained by the deletion of a small number of nucleotides with a simultaneous insertion of a few nucleotides at the same site. This type of mutation was reported previously in wild-type Muta® mice (*17*) and gpt delta transgenic mice (*18*) after irradiation. The multiple mutations we encountered can be grouped into two categories: (1) two or three changes within 14 nucleotides and (2) two alterations observed separately with a distance of 558 bp or more. Interestingly, the latter class of mutation was found only in irradiated *Ku70*⁻/⁻ mice (four cases) and not in unirradiated mice or irradiated *Ku70*-proficient mice. We found 188 independent mutations in irradiated *Ku70*-pro-